Effects of varied nitrate and phosphate supply on polysaccharidic and proteinaceous gel particle production during tropical phytoplankton bloom experiments

Engel, A., Borchard, C., Loginova, A., Meyer, J., Hauss, H. and Kiko, R.

GEOMAR Helmholtz Centre for Ocean Research, 24105 Kiel, Germany

Keywords: Transparent exopolymer particles (TEP), Coomassie stainable particles (CSP), mesocosms, N:P ratio, dissolved organic carbon (DOC), dissolved organic nitrogen (DON)

Abstract

Gel particles such as the polysaccharidic transparent exopolymer particles (TEP) and the proteinaceous Coomassie stainable particles (CSP) play an important role in marine biogeochemical and ecological processes like particle aggregation and export, or microbial nutrition and growth. So far, effects of nutrient availability or of changes in nutrient ratios on gel particles production and fate are not well understood. The Tropical Ocean includes large oxygen minimum zones, where nitrogen losses due to anaerobic microbial activity result in a lower supply of nitrate relative to phosphate to the euphotic zone. Here, we report of two series of mesocosm experiments that were conducted with natural plankton communities collected from the Eastern Tropical North Atlantic (ETNA) close to Cape Verde in October 2012. The experiments were performed to investigate how different phosphate (Experiment 1, *Varied P:* 0.15 - 1.58 μmol L^{-1}) or nitrate (Experiment 2, *Varied N:* 1.9 - 21.9 μmol L^{-1}) concentrations affect the abundance and size distribution of TEP and CSP. In the days until the bloom peak was reached, a positive correlation between gel particle abundance and Chl *a* concentration was determined, linking the release of dissolved gel precursors and the subsequent formation of gel particles to autotrophic production. After the bloom peak, gel particle abundance remained stable or even increased, implying a continued partitioning of dissolved into particulate organic matter after biomass production itself ceased. During both experiments, differences between TEP and CSP dynamics were observed; TEP were generally more abundant than CSP. Changes in size distribution indicated aggregation of TEP after the bloom, while newly formed CSP decomposed. Abundance of gel particles clearly increased with nitrate concentration during the second experiment, suggesting that changes in [DIN]:[DIP] ratios can affect gel particle formation with potential consequences for carbon and nitrogen cycling as well as food web dynamics in tropical ecosystems.

1. Introduction

Ecosystem productivity in the surface ocean is largely controlled by the availability of inorganic nutrients. The Redfield ratio describes a constant molar ratio of C:N:P of 106:16:1 and associates the relative elemental composition of seawater to that of marine organisms (Redfield, 1958; Redfield et al., 1963). It provides a widely used basis for the calculation of elemental fluxes in marine food webs and biogeochemical cycles (Sarmiento and Gruber, 2006; Sterner and Elser, 2002). On a regional or temporal scale, however, strong deviations of cellular composition from the Redfield ratio were reported (Fraga, 2001; Geider and LaRoche, 2002), and related to the physiological state of cells (Rhee, et al. 1978; Goldman et al., 1979; Falkowski, 2000; Borchard et al., 2011; Franz et al., 2012a), differences in growth strategies (Klausmeier et al., 2004; Mills and Arrigo, 2010; Franz et al. 2012b) and changes in community structure (Sommer et. al., 2004; Hauss et al., 2012). With regard to CO_2 uptake and organic matter production, variations in element stoichiometry of cells have been linked to carbon overconsumption - a particular increase in carbon assimilation relative to the uptake of nitrogen and phosphorous (Toggweiler, 1993; Schartau et al., 2007), when photosynthesis proceeds, while cell division and growth are hampered due to nutrient limitation (Wood and van Valen, 1990).

A fraction of this 'excess carbon' is released from phytoplankton cells in the form of dissolved organic carbon (DOC). DOC release occurs during all stages of phytoplankton growth (Fogg, 1983; Mague et al., 1980; Bjørnsen, 1988). In natural communities, the percentage of extracellular release typically ranges between 10-20% (Baines and Pace, 1991; Nagata, 2000). Depending on their nutrient status, however, marine phytoplankton cells can release up to 80% of primary production as DOC (Sharp, 1977; Mague, 1980; Fogg, 1983; Bjørnsen, 1988). Thereby,

the extent and composition of freshly produced DOC is affected by various environmental factors, such as temperature, CO_2 concentrations and nutrient supply (Thornton, 2009; Engel et al., 2011; Borchard and Engel, 2012). Abiotic factors influencing DOC production concomitantly define its fate in the global carbon cycle. DOC can either be transferred back to CO_2 by microbial degradation and respiration (Azam, 1983; Ducklow et al. 1986; del Giorgio and Duarte, 2002), or it can be transformed into particulate organic carbon (POC), either through uptake by organisms, or by abiotic assembly and coagulation into gel particles (Alldredge et al., 1993; Chin et al., 1998; Engel et al., 2004a; Verdugo et al., 2004).

The formation of gel particles thus represents an abiotic pathway of repartitioning dissolved organic matter (DOM) into particulate organic matter (POM). To date, mostly two types of gel particles have been described in seawater: transparent exopolymer particles (TEP) that are rich in carbon and mainly originate from dissolved polysaccharides, and Coomassie stainable particles (CSP) that are rich in nitrogen and assumed to form from proteinaceous compounds (Alldredge et al., 1993; Long and Azam, 1996; Engel, 2009; Cisternas-Novoa et al., 2015). Ubiquitous in the ocean, numerical abundances of TEP and CSP around 10^6 L^{-1} have been reported, with higher abundances (10^8 L^{-1}) during phytoplankton blooms (Long and Azam, 1996; Passow, 2002; Galgani et al., 2014). It has been shown that the rate of TEP formation during phytoplankton blooms is controlled by the release rate of dissolved polysaccharides (Engel et al., 2004a). TEP abundance often increases at times when phytoplankton growth becomes nutrient limited, either by nitrogen (Corzo et al., 2000; Pedrotti et al., 2010) or by phosphorus (Borchard and Engel, 2011). In addition to phytoplankton, often considered as main source of dissolved gel precursors, bacteria can significantly contribute to the DOM pool and therewith to TEP and CSP formation

(Radic et al., 2006; Vadstein et al., 2012). TEP play an important role in the formation of particle aggregates and therewith can enhance carbon export fluxes in marine systems (Passow et al., 2001; Engel et al., 2014). Due to the high carbohydrate content, high abundance of TEP can increase C:N ratios of suspended and sinking particles in the ocean (Engel et al., 2002, Schneider et al., 2004; Schartau et al., 2007).

It has been suggested that CSP and TEP are different particles, as their spatial and temporal occurrence in the ocean can be quite different (Cisternas-Novoa et al., 2015). Compared to TEP, much less is known for processes controlling CSP formation. However, it can be assumed that dissolved precursor concentration and quality are affecting CSP formation in a similar way that DOC precursors are affecting TEP formation (Cisternas-Novoa et al., 2014). Thus, CSP formation may be part of the extracellular cycling of organic nitrogen, i.e. CSP precursors are released by microorganisms into the dissolved organic nitrogen (DON) pool and repartitioned into particles by abiotic gel particle formation. Nitrogen is often considered to be a temporarily limiting element of biomass production in marine ecosystems, favouring auto- and heterotrophic nitrogen fixation (Gruber and Sarmiento, 1997; Deutsch et al., 2007). A labile, extracellular fraction of organic nitrogen in the form of CSP thus represents a potentially important source of nutrition. Moreover, extracellular particulate nitrogen included in CSP may erroneously be attributed to the cellular nitrogen pool and may hence disguise the real nitrogen cell quota. Thus, a better knowledge on CSP formation and of the factors controlling CSP abundance may greatly improve our understanding of nitrogen cycling in marine ecosystems. So far it is unknown, how much CSP contribute to variable stoichiometry of POM, but we can expect that changes in N:P

115 nutrient stoichiometry favouring organic nitrogen release also support higher CSP abundance,
116 potentially increasing the nitrogen fraction in POM.

117 In this study, we investigated how gel particle formation is affected by different nitrate and
118 phosphate concentrations during mesocosm bloom experiments with natural plankton
119 communities collected from surface waters of the Eastern Tropical North Atlantic (ETNA), close
120 to Cape Verde. At this site, surface waters are often depleted in nutrients (Hauss et al., 2013).
121 Coastal upwelling, N_2- fixation or deposition of Aeolian dust represent prevalent pathways of
122 nutrient, particularly inorganic nitrogen, supply to nutrient depleted surface waters (Baker et al.,
123 2007; Hansell et al., 2004; Hauss et al., 2013). On the other hand, anoxic mesoscale eddies have
124 been described recently in surface waters around Cape Verde, potentially leading to enhanced
125 nitrogen losses (Karstensen et al., 2014). Thus, pelagic communities in the euphotic zone of the
126 ETNA are occasionally exposed to nutrient pulses with different $[NO_3^-]$: $[PO_4^{3-}]$ ratios in surface
127 waters.

128 Understanding the impact of changes in nutrient stoichiometry on phytoplankton communities in
129 the Tropical Ocean may also help to better estimate consequences of suboxia on ecosystem
130 productivity and biogeochemical cycling. Coastal boundary upwelling systems in the ETNA and
131 Eastern Tropical North Pacific (ETNP) include some of the largest oxygen minimum zones
132 (OMZ) in the ocean (<20-45 µmol O_2 kg^{-1}) (Gilly et al., 2013). Although they comprise only a
133 small fraction of the global ocean by volume, they nevertheless play a pivotal role in controlling
134 the oceans nutrient regimes (Lam and Kuypers, 2011). A profound loss of the oceanic nitrate
135 stock was suggested to occur in OMZs (Gruber and Sarmiento, 1997, Codispoti et al., 2001) due
136 to microbial processes, such as heterotrophic denitrification and anaerobic ammonium oxidation
137 (anammox) (Codispoti and Richards, 1976; Kuypers et al., 2005). As a consequence, the $[NO_3^-]$:

138 [PO_4^{3-}] stoichiometry of upwelling water masses above OMZs with strong nitrogen loss often
139 deviate from the canonical Redfield ratio of 16 (Deutsch et al., 2007). Because global climate
140 change may lead to an expansion of OMZ, particularly in the Atlantic and Pacific Ocean
141 (Stramma et al., 2008), future changes in surface ocean nutrient cycling are to be expected.
142 Our experiments aimed to identify effects of varied nutrient supply and stoichiometry on the
143 abundance and size distribution of TEP and CSP, their dissolved precursors and the potential
144 impact on carbon and nitrogen cycling.

145

2. Methods

2.1 Setup of the mesocosms

Two 8-day mesocosm experiments were conducted in October 2012 at the Instituto Nacional de Desenvolvimento das Pescas (INDP), Mindelo, Cape Verde. Surface water was collected with RV *Islândia* south of São Vicente (16°44.4'N, 25°09.4'W) using four 600L containers. Surface water was collected in the night of the 01.10.2012/02.10.2012 (first experiment) and 11.10.2012/12.10.2012 (second experiment). Sixteen mesocosm (MK) bags were placed in four flow-through water baths and shaded with blue, transparent lids to approximately 20% of surface irradiation. Mesocosm bags were filled from the containers by gravity, using a submerged hose to minimize bubbles. A mesh to filter out zooplankton was not used in order to avoid changes of the community composition as well as breakage of delicate cells. The accurate volume inside the individual bags was calculated after addition of 1.5 mmol silicate and measuring the resulting silicate concentration. The volume ranged from 106 to 145 L. In order to keep the temperature constant, all mesocosms were evenly distributed between four water baths, the temperature of which was maintained at 25.9 - 28.7°C using water from the bay close to the experiment site. Daily sampling was conducted between 9.00 a.m. and 10.30 a.m. with a 10L beaker completely rinsed with ultra-pure water. Between 5.5 and 7 liters were sampled from each mesocosm at the surface and used for all further analyses. The mesocosms were gently mixed prior to sampling to obtain representative samples for the entire mesocosm

The experimental manipulation comprised additions of different amounts of nitrate (NO_3^-) and phosphate (PO_4^{3-}) at day 1 of the experiment. Treatment identifications specifying micromolar target concentrations of NO_3^- and PO_4^{3-} are given in table 1. Nutrient concentrations before

168 nutrient addition were below the detection limit for NO_3^-, NO_2 and PO_4^{3-} while only traces of
169 NH_4 (<0.08 µmol L^{-1}) were determined.

170 In experiment 1 (referred to as *Varied P* in the following), the PO_4^{3-} supply was changed at
171 constant NO_3^- supply, yielding a range of 0.25-1.75 µmol L^{-1} PO_4^{3-} at 12.0 µmol L^{-1} NO_3^- (Table
172 1) for 13 tanks. Two additional mesocosms were set to 1.10 µmol L^{-1} PO_3^{4-} at 6.35 and 17.65
173 µmol L^{-1} NO_3^-, respectively, representing low and high NO_3^- treatments. One mesocosm (MK 5)
174 received erroneous filling during the *Varied P* experiment and was excluded from data
175 evaluation. Realized concentrations of PO_3^{4-} and NO_3^- inside the mesocosms slightly deviated
176 from target values (Table 1), which may be due to fast uptake, or to underestimation of water
177 volume. Initial $[NO_3^-]$: $[PO_4^{3-}]^-$ during *Varied P* covered a range of 6.7 – 77, with ratios similar to,
178 or smaller than the Redfield value, in 11 out of 15 mesocosms, suggesting non-P-limiting
179 conditions in the majority of mesocosms during the first experiment. .
180 During experiment 2 (referred to as *Varied N* in the following), initial NO_3^- concentration was
181 varied at relatively constant PO_3^{4-} concentration, yielding a target range of 2.0 - 20.0 µmol L^{-1}
182 NO_3^- at 0.75 µmol L^{-1} PO_4^{3-} in 12 out of 16 MKs (Table 1). In addition, two low and two high
183 PO_3^{4-} treatments at low and high NO_3^- were realized. The realized nutrient concentrations
184 deviated only slightly from target values. $[NO_3^-]$: $[PO_4^{3-}]$ during *Varied N* therewith covered a
185 range of 3.3 – 84 with ratios of > 16, in 9 out of 16 mesocosms suggesting non-N-limiting
186 conditions in the majority of mesocosms during the second experiment.Two nutrient treatments
187 were realized in both experiments: 12.0N/0.75P with 4 replicates during *Varied P* and 3
188 replicates during *Varied N*, and 6.35N/1.10P with 1 mesocosm during each experiment.
189

190 **2.2 Analytical methods**

2.2.1. Inorganic nutrient

The dissolved inorganic nutrients nitrate (NO_3^-), nitrite (NO_2^-) and phosphate (PO_4^{3-}) were determined from 10mlsamples.

Duplicate measurements were carried out within four hours after sampling using a Quattro Autoanalyzer according to Grasshoff et al. (1999). Detection limits of nutrients were 0.01 µmol L^{-1} for NO_2^- and PO_4^{3-}, and 0.03 µmol L^{-1} for NO_3^-.

2.2.2 Gel particles

For transparent exopolymer particles (TEP) and for Coomassie stainable particles (CSP), duplicate samples of 20-80 ml were gently (< 150 mbar) filtered onto 25 mm nuclepore membrane filters (0.4 µm pore size, Whatman Ltd.). Samples were stained with either 1ml of pre-filtered (<0.2 µm) Alcian Blue solution (Allredge et al., 1993) or 1ml of pre-filtered (<0.2 µm) Coomassie Brilliant Blue solution (Long and Azam, 1996). After a staining time of approximately 4s (Alcian Blue) or 30s (Coomassie Brilliant Blue), the excessive dye was removed by rinsing the filter with several millilitres of MilliQ water. Blank filters were prepared from the same MilliQ water. No samples for gel particles have been taken during *Varied P* on day 3 and 4 due to a break-down of the ultra-pure water system.

Each filter was placed on the white side of a semi-transparent glass slide (CytoClear, Poretics Corp., Livermore, US) and stored frozen (-20°C) until microscopic analysis. Abundance, area and size frequency distribution of TEP and CSP in the size range 1-760 µm were determined after Engel (2009) using a light microscope (Zeiss Axio Scope A.1) connected to a camera (AxioCAM Mrc). Filters were screened at 200x magnification. 30 pictures were taken randomly from each filter in two perpendicular cross sections (15 pictures each; resolution 1040 x 1040 pixel, 8-bit color depth). Image analysis software WCIF ImageJ (Version 1.44, Public Domain, developed at

215 the US National Institutes of Health, courtesy of Wayne Rasband, National Institute of Mental
216 Health, Bethesda, Maryland) was used to semi-automatically analyse particle numbers and area.
217 The size frequency distribution of gel particles can be described by:
218

$$dN / d(d_p) = k d_p^{\delta} \quad (1)$$

220

221 where dN is the number of particles per unit water volume in the size range d_p to $[d_p + d(d_p)]$ with
222 d_p being the equivalent spherical diameter (ESD), k is a constant that depends on the total number
223 of particles per volume, and δ ($\delta < 0$) describes the spectral slope of the size distribution. The less
224 negative δ the greater is the fraction of larger gels. Both, δ and k were derived from regressions of
225 $\log[dN/d(d_p)]$ versus $\log[d_p]$ (Mari and Kiørboe, 1996). The value δ is related to the slope of the
226 cumulative size distribution $N = a d_p^{\beta}$ by $\delta = \beta + 1$. To determine δ, data for CSP and TEP were fitted
227 over the size range 1.05-14.14 µm ESD. Median size (ESD) of TEP and CSP were determined
228 over the whole size range (1-760 µm).
229 The carbon content of TEP (TEP-C) was estimated after Mari (1999) using the size dependent
230 relationship:
231

232 $$TEP\text{-}C = a \, \Sigma_i \, n_i \, r_i^D \quad (2)$$

233

234 with n_i being the number of TEP in the size class i and r_i the mean equivalent spherical radius of
235 the size class. The constant a = 0.25 * 10^{-6} (µg C) and the fractal dimension of aggregates
236 D=2.55 were proposed by Mari (1999). In order to relate TEP-C to POC and TOC, data are given
237 as µmol L^{-1}.

238

239 **2.2.3 Dissolved organic carbon and nitrogen**

240 Duplicate samples for DOC (20 ml) were filtered through pre-combusted GF/F filters (450°C for
241 5 hours) and collected in pre-combusted glass ampoules (450°C for 5 hours). Samples were
242 acidified with 80 µl of 85% phosphoric acid, flame sealed and stored at 4°C in the dark until
243 analysis. DOC samples were analysed by applying the high-temperature catalytic oxidation
244 method (TOC -VCSH, Shimadzu) after Sugimura and Suzuki (1988). The instrument was
245 calibrated every 8-10 days by measuring standard solutions of 0, 500, 1000, 1500, 2500 and 5000
246 µg C L^{-1}, prepared from a potassium hydrogen phthalate standard (Merck 109017). Every
247 measurement day, ultrapure (MilliQ) water was used for setting the instrument baseline, followed
248 by the measurement of deep-sea water with known DOC concentration (Dennis Hansell,
249 RSMAS, University of Miami) to verify results. Additionally, two internal standards with DOC
250 within the range of found in samples were prepared each measurement day using a potassium
251 hydrogen phthalate (Merck 109017). DOC concentration was determined in each sample from 5
252 to 8 injections.

253 Simultaneously with DOC, total dissolved nitrogen (TDN) was determined using the TNM-1
254 detector on the Shimadzu analyzer. Dissolved organic nitrogen (DON) was calculated from TDN
255 by subtraction of NO_3^- and NO_2^- concentrations.

256

257 **2.2.4 Chlorophyll *a***

258 Samples (0.5-1 L) for chlorophyll a (Chl *a*) were vacuum-filtered (<200 mbar) onto Whatman
259 GF/F filters (25mm), 1 ml ultrapure water was added and the filters were frozen at -20°C for at
260 least 24 hours. Subsequently, 9 ml acetone (100 %) was added to each sample and the

261 fluorescence was measured with a Turner Trilogy fluorometer, which was calibrated with a Chl *a*
262 standard (*Anacystis nidulans*, Walter CMP) dilution series. Chl *a* concentrations were calculated
263 according to Parsons et al. (1984).

264

265 **2.2.5 Bacterial abundance**

266 Bacterial cell counts were obtained by flow cytometry (FACScalibur, Becton Dickinson, San
267 Jose, CA, USA). Samples (5ml) were fixed with formaldehyde (2% final concentration), frozen at
268 -80°C and transported to the home laboratory. Samples were diluted 1:3, stained with SYBR
269 Green I (Molecular Probes) and measured at a flow rate of 11.0 µl min^{-1}.

270

271 **2.2.6 Particulate organic carbon and nitrogen**

272 For analyses of particulate organic carbon (POC) and particulate nitrogen (PN) water samples
273 (0.5-1 L) were filtered onto pre-combusted (450°C for 5 hours) Whatman GF/F filters (25mm,
274 0.7 µm) under low pressure (<200 mbar). Filters were frozen at -20°C and stored until analysis.
275 Prior to analysis, filters were acid fumed (37% HCl for 24 hours) in order to remove inorganic
276 carbon and dried at 40°C for 24 hours. Subsequently, filters were wrapped in tin cups (8 × 8 × 15
277 mm), combusted and analyzed according to Sharp (1974) using an elemental analyzer (Euro EA).

278

279 **2.3 Data analysis**

280 Differences in terms of nutrient manipulation and course of the experiments were statistically
281 tested by multiple comparison (Holm-Sidak-method) or by two-way ANOVA with factors being
282 the treatment identification (Table 1) and day of the experiment, respectively. To determine a
283 potential effect of the nutrient treatment, the mean deviation (*MD*) of a component in a

284 mesocosm was calculated as mean of daily deviations. Those were calculated for each sampling
285 day by subtracting the mean value of all mesocosms at that day from the value of the individual
286 mesocosm of the same day. For each experiment, *MD*-values were correlated to the initial (day 1)
287 nutrient concentration. The overall significance level was $p<0.05$. Statistical tests were
288 performed using Sigma Plot 12.0 (Systat).
289

3. Results

3.1 Phytoplankton bloom and nutrient development

The development of phytoplankton blooms during the mesocom experiments and the build-up of particulate matter are described in more detail in Meyer et al. (2015) and are summarized here only briefly.

Before nutrient addition (day 0), Chl *a* concentration was on average 0.38 ± 0.09 µg L^{-1} in all mesocosms of *Varied P* and hence higher than at the start of *Varied N* with 0.18±0.05 µg L^{-1} (Table 1). As long as nutrients were replete, bloom development was similar in all mesocosms within each experiment (Fig. 1a-f). However, during *Varied P* most mesocosms reached maximum Chl *a* concentrations, i.e. bloom peak, on day 5 and thus one day earlier than during *Varied N* (Fig. 1 a, b). Maximum Chl *a* concentration ranged between 2.1 and 3.3 µg L^{-1} during *Varied P* and between 2 and 10 µg L^{-1} during *Varied N*. Hence, during *Varied N* higher concentrations of Chl *a* were determined as well as a higher variability among mesocosms. During both experiments mean deviations (MD) of Chl *a* concentration in the different mesocosms were correlated to the concentration of the initial nutrient varied, i.e. PO_4^{3-} during *Varied P* and NO_3^- during *Varied N*, although the response was much stronger during *Varied N* (Table 2). The phytoplankton biomass composition was dominated by diatoms (data not shown). Diazotrophic bacteria of the genus *Trichodesmium* were more present in the initial waters of *Varied P*, while proteobacterial diazotrophs were more abundant in *Varied N* (Meyer et al., 2015).

Bacterial abundance was not determined before nutrient addition, but data from day 2 showed higher abundance in mesocosms of *Varied N* with 8.37 x 10^5 ± 9.80 x 10^4 ml^{-1} compared to 5.26x10^5 ± 5.48 x 10^4 ml^{-1} for *Varied P*. During the first four days of both experiments, cell

313 numbers remained relatively stable or even decreased slightly (Fig. 1 c, d). After day 5, cell
314 numbers increased in all mesocosms and strongly differed between treatments. During *Varied P*,
315 different PO_4^{3-} addition could not significantly explain differences in bacterial abundance (Table
316 2). Instead, highest abundances in the bloom phase were reached in the 'centrepoint' treatment
317 (12.0N/0.75P), with a maximum value of $2.4x10^6 \pm 7.1x10^5$ ml^{-1} on day 6 compared to $2.3x10^6 \pm$
318 $7.1x10^5$, $1.5x10^6 \pm 3.0x10^5$ and $1.7x10^6 \pm 8.4x10^5$ ml^{-1} in treatments 12.0N/0.25P, 12.0N/1.25P
319 and 12.0N/1.75P, respectively. During *Varied N*, bacterial abundances were positively influenced
320 by NO_3^- input (Table 2). At the end of the experiment (day 8) $1.6x10^6 \pm 4.7x10^5$ and $2.3x10^6 \pm$
321 $5.4x10^5$ ml^{-1} cells were observed in the high NO_3^- treatments 20.0N/0.75P and 12.0/0.75P,
322 respectively, compared to $8.1x10^5 \pm 1.4x10^5$ and $1.0x10^6 \pm 1.5x10^5$ ml^{-1} in 2.0N/0.75P and
323 4.0N/0.75P, respectively.

324 Initial concentrations of POC were 13.6±3.8 µmol L^{-1} and 11.9±1.9 µmol L^{-1} during *Varied P*
325 and *Varied N*, respectively (Table 1). During both experiments, concentrations increased steadily
326 until day 6 and remained relatively stable thereafter (Fig. 1e, f). POC concentrations during
327 *Varied P* were up to 73 µmol L^{-1} (17.65N/1.10P), but not related to the initial PO_4^{3-} addition. In
328 contrast, build-up of POC was more pronounced during *Varied N* with values up to 102±18 µmol
329 L^{-1} determined in treatments with the highest initial NO_3^- supply (20.0N/0.75P) and indicated a
330 clear correlation to the initial NO_3^- treatment (Table 2).
331
332 Along with plankton growth, inorganic nutrient concentrations declined (Fig. 2). During *Varied P*,
333 PO_4^{3-} was exhausted on day 5 in the treatments with the lowest initial PO_4^{3-} supply and the
334 highest initial $[NO_3^-]$: $[PO_4^{3-}]$ ratio of 74, i.e. 12.0N/0.25P. In all other treatments, PO_4^{3-} depletion
335 was reached later during the experiment, except for the highest PO_4^{3-} treatment (12.0N/1.75P), in

which PO_4^{3-} remained >0.3 µmol L^{-1} until the last experimental day. During the same experiment, NO_3^- concentrations fell below the detection limit of 0.03 µmol L^{-1} in some of the mesocosms after day 5, but were not depleted in 12.0N/0.25P. During *Varied N*, NO_3^- was exhausted on day 5 in the low N supply mesocosms (2.00N/0.75P and 4.00N/0.75P). On day 6, NO_3^- was still available in treatments with an initial nitrate supply > 12 µmol L^{-1}, and on day 8 NO_3^- was only available in 17.65N/0.40P, the mesocosms with the highest $[NO_3^-]$: $[PO_4^{3-}]$ ratio of 84. After the bloom, PO_4^{3-} was below the detection limit in 9 out of 16 mesocosms having $[NO_3^-]$:$[PO_4^{3-}]$ ratios >10.

3.2 Dissolved organic carbon (DOC) and nitrogen (DON)

Averaged for all mesocosms, initial (day 1) DOC concentration was very similar for *Varied P* (95±5 µmol C L^{-1}) and *Varied N* (96±4 µmol C L^{-1}) (Table 1). Throughout both experiments, DOC concentrations increased steadily after day 2, except for day 5, when a slight decrease was observed in most mesocosms (Fig. 3a, b). For *Varied P*, accumulation of DOC with respect to initial concentration (day 1) (ΔDOC) was observed, ranging from 18.8±6.7 µmol L^{-1} (12.0N/0.25P) to 44.0±12.0 µmol L^{-1} (12.0N/0.75P). During *Varied N*, ΔDOC increased also in the course of the experiment with highest values observed at the end of the experiment, ranging from 12.1±1.1 µmol L^{-1} DOC in the treatment with the lowest nitrate supply (2.0N/0.75P) to 74.4±16.6 µmol L^{-1} in 12.0N/0.75P 75, the same treatment that yielded highest ΔDOC during *Varied P*. MD of DOC were not significantly correlated to the initial PO_4^{3-} supply during *Varied P* , but to the initial NO_3^- supply during *Varied N* (p<0.005), indicating a general dependence of DOC accumulation on NO_3^- stocks (Table 2).

On day 1, DON concentration (day 1) was 8.8 ± 1.1 and 11 ± 1.5 µmol L^{-1} for mesocosms of *Varied P* and *Varied N,* respectively. In both experiments, DON concentration decreased after nutrient addition (Fig. 3c, d). During *Varied P*, ΔDON was negative in some of the mesocosms until the Chl *a* maximum on day 5. Values increased slowly between days 6 and 7 before a clear increase was determined for all mesocosms on day 8 with ΔDON accumulation ranging between 1.9 and 5.9 µmol L^{-1} (Fig. 3c). During *Varied N*, a clear accumulation of DON was not observed, yielding values of ΔDON of -6.0 to 4.8 µmol L^{-1} at the end of the experiment. On day 8 of both experiments, highest and lowest ΔDON was determined in the treatments with the highest and lowest initial NO_3^- supply at identical PO_4^{3-} supply, respectively. A significant correlation between the initial PO_4^{3-} or NO_3^- supply and DON accumulation, however, was not determined (Table 2).

Both, increasing DOC and decreasing DON concentrations resulted in a rise of molar [DOC]:[DON] ratios until the bloom peak during both experiments (data not shown). During *Varied P* [DOC]:[DON] ratios were initially 10.1±0.92, averaged for all mesocosms and ranged between 7.7 and 31 throughout the experiment, with highest values being observed just before the bloom peak. During *Varied N*, [DOC]:[DON] ratios started at 9.1±1.1 and ranged between 6.8 and 34 throughout the experiment, with highest values also observed shortly before the bloom peak on day 6.

3.3 Gel particle abundance

Averaged for all mesocosms, initial (day 1) TEP numerical abundance was 0.97 ± 0.64 x 10^7 L^{-1} for *Varied P* and steadily increased to highest values between 5.9 x 10^7 and 1.5 x 10^8 L^{-1} until the end of the study (Fig. 4a). TEP total area behaved similar to TEP numerical abundance;

382 values increased from an initial 4.46 ± 2.36 x 10^7 µm² L^{-1} to values between 3.9 x 10^8 and 7.9x
383 10^8 µm² L^{-1} on day 8 (data not shown). Variation of initial NO_3^- concentrations during *Varied N*
384 induced clearly stronger responses in TEP formation than variation of initial PO_4^{3-} concentration
385 (Fig. 4b). From an averaged 1.07 ± 0.34 x 10^7 L^{-1}, TEP abundance increased until day 8 to values
386 of 1.1 x 10^8 – 2.8 x 10^8 L^{-1}. While initial numbers were in a comparable range for both
387 experiments, the maximum TEP abundances (day 8) during *Varied N* were about twice as high as
388 during *Varied P*. The same holds for TEP total area: Initial averaged values were only slightly
389 higher (5.04±1.43 x 10^7 µm² L^{-1}) than initial values during *Varied P*, but highest values more than
390 doubled on day 8 during *Varied N*, yielding 9.6 x 10^8 -1.6 x 10^9 µm² L^{-1} (data not shown).
391
392 During both experiments, TEP numbers and total area increased similarly in all treatments until
393 the Chl *a* maximum. From day 6 onwards, however, distinct differences emerged between
394 treatments, particularly during *Varied N*. Here, TEP abundance was significantly higher in the
395 highest NO_3^- treatment (20.0N/0.75P) compared to treatments amended with lower nitrate supply
396 (2.0N/0.75P; $p<0.001$, 4.0N/0.75P; $p<0.005$, 6.0N/1.03P; $p<0.05$). On day 7, TEP numbers in
397 20.0N/0.75P reached their maximum and were significantly higher than in all other treatments
398 ($p<0.001$), where TEP numbers continued to increase on day 8. Like TEP numbers, TEP total
399 area was also significantly larger in the highest NO_3^- treatment (20.0N/0.75P) compared to
400 2.0N/0.75P and 6.0N/1.03P ($p<0.01$) showing a clear stimulation of TEP formation at higher
401 nitrate levels.
402 For *Varied P*, initial PO_4^{3-} concentration had on average no significant effect on MD of TEP
403 abundance (Table 2). In contrast, a significant positive relationship between MD of TEP
404 abundance and initial NO_3^- supply was determined during *Varied N* ($p<0.001$). This relationship,
405 however, reversed when MD of Chl a normalized TEP concentration were considered, indicating

406 that a relatively higher fraction of newly fixed organic carbon was partitioned into TEP at lower
407 nitrate supply on a cellular level ($p<0.001$; data not shown).

408

409 Similar to TEP, CSP abundance and total area increased steadily over time during both
410 mesocosm experiments, albeit CSP were generally less abundant than TEP (Fig. 4c, d). From an
411 initial mean value of 1.06 ± 0.61 x 10^6 L^{-1} during *Varied P,* CSP numerical abundance increased
412 to 4.2 x 10^6 to 1.0 x 10^7 L^{-1} on day 8. Highest CSP abundance was determined in the treatment
413 with the highest nitrate supply (17.65N/1.10P), where CSP total area of initially 1.5 ± 0.5 x 10^7
414 µm² L^{-1} increased to 4.5 x 10^7 - 1.2 x 10^8 µm² L^{-1} on day 8. Similar to TEP, a much stronger
415 increase in CSP abundance was observed during *Varied N*. Here, CSP numbers increased from an
416 initial average of 1.63 ± 0.48 x 10^6 L^{-1}, to highest values of 1.4 x 10^7 - 2.8x 10^8 L^{-1} on day 7 (Fig.
417 5d); more than double the amount observed during *Varied P*. Again, highest CSP abundances
418 were determined in replicate treatments of highest NO_3^- supply (20.0N/0.75P) yielding 2.7±0.1 x
419 10^7 L^{-1}.

420

421 Analysis of variance for data obtained on day 7 revealed significantly higher CSP abundances in
422 20.0N/0.75P compared to 2.0N/0.75P ($p<0.001$), 4.0N/0.75P ($p<0.001$) and 6.35N/0.40P
423 ($p<0.05$), indicating a stimulation of CSP formation at elevated initial NO_3^- concentrations. This
424 is in accordance with a highly significant correlation of MD of CSP abundance and initial NO_3^-
425 concentrations ($p< 0.001$, Table 2). Findings for CSP numbers are reflected in CSP total area:
426 highest values were also observed for the high NO_3^- treatment (20.0N/0.75P; 213±21 x 10^6 µm² L^{-1})
427 with values significantly larger than in 2.0N/0.75P ($p<0.005$), 4.0N/0.75P ($p<0.001$),
428 6.35N/0.40P ($p<0.001$), 17.65N/1.10P ($p<0.05$) and 12.0N/0.75P ($p<0.005$) (data not shown). In

429 contrast to TEP abundance, CSP number declined in most treatments on day 8 of *Varied N*
430 (except for 12.0N/0.75P; only MK 1, 6.35N/0.40P and 4.0N/0.75P; only MK 11).
431
432 **3.4. Gel particle size distributions**
433 At the beginning of the study, median values for TEP equivalent spherical diameter (ESD) were
434 almost identical for *Varied P* and *Varied N,* yielding 1.78 ± 0.12 and 1.79 ± 0.08 µm ESD,
435 respectively. Except for days 6 and 8, median size of TEP was steadily increasing over time in
436 *Varied P*, with largest particles occurring in 6.35N/1.10P, 12.0N/1.75P and 12.0N/1.25P on day 7
437 (2.28 - 2.30 µm ESD). On day 8, median TEP size was slightly smaller again and similar in all
438 treatments ranging between 1.80 and 2.26 µm ESD. During *Varied N*, size of TEP remained
439 relatively constant between days 1-4 and then increased until the Chl *a* maximum. After the
440 bloom peak, median TEP size further increased until day 6 yielding values between 2.5 and 1.9
441 µm ESD at the end of the experiment.
442 Spectral slopes describe the size frequency distribution of particles with more negative values
443 indicating relatively more small particles (Fig. 5) and mirrored changes in the median ESD of
444 both types of gel particles during both experiments. Changes in size frequency distribution of
445 TEP were observed for *Varied P* and *Varied N*, with slope values (δ) becoming significantly
446 smaller during the first half of both experiments ($p<0.001$; multiple comparison, Holm-Sidak)
447 (Fig. 6). Average slopes on day 1 were very similar for *Varied P* and *Varied N*, yielding δ=-1.81
448 ± 0.12 and δ=-1.81 ± 0.11, respectively. Slopes increased to average -1.44±0.06 (*Varied P*) and -
449 1.38 ± 0.06 (*Varied N*) on day 8 of both experiments suggesting a relative shift from smaller to
450 larger TEP (Fig. 6a, b).
451

Slightly smaller than TEP, median CSP size was on average 1.37 ± 0.06 µm ESD at the beginning of *Varied P*, and increased to values between 1.13 and 1.78 µm ESD until the end of the experiment (Fig. 6c). During *Varied N,* median CSP size increased between day 1 (1.36 ± 0.09 µm ESD) and day 4 (1.34-1.85 µm ESD). In contrast to median TEP size, median CSP decreased towards the end of the experiments and ranged between 1.18 and 1.71 µm ESD on day 8. During *Varied P*, a large variability of δ values was observed for CSP size distribution on day 1. To estimate changes in size distribution during this experiment, data evaluation of CSP slopes was started on day 2 (Fig. 6c), when CSP size distribution was more similar between mesocosms. Like for TEP, development of CSP spectral slopes during this study mirrored the change in median ESD size of particles. Averaged for all mesocosms, δ=-1.40 ± 0.14 was obtained on day 2 of *Varied P* increasing steadily to -1.24 ± 0.23 until day 8. The size frequency distribution of CSP during *Varied P* was not affected by the initial nutrient supply. For *Varied N*, initial slopes also scattered on day 1, however not as strong as for initial values for *Varied P*. Initial averaged slopes for all mesocosms were -1.64 ± 0.28 (Fig. 6d). During days 2-4, the overall development shows a relative increase in the slope of the size distribution during the onset of the bloom. Highest values of δ=-0.84 coincided with the largest median ESD of CSP on day 4. At the time of the Chl *a* maximum, slopes became more negative, revealing higher abundance of relatively small particles. Multiple comparison (Holm-Sidak) tests revealed significantly larger slopes for days 2 to 4, compared to days 1, 6, 7 and 8 (p<0.010). The increase in abundance of smaller CSP continued during the bloom decay and was most pronounced in 2.0N/0.75P and 4.0N/0.75P, the treatments with the lowest initial NO_3^- supply.

3.5. Differences between two mesocosm experiments - a case of treatment effects?

475 Although the development of gel particle abundance was rather similar for TEP and CSP during
476 both experiments, particularly until the bloom peak, abundance of gel particles was clearly higher
477 during the second mesocosm experiment, *Varied N,* compared to *Varied P* (Fig. 4). Moreover,
478 during *Varied N,* CSP increased relatively more than TEP and showed a unique change of size
479 distributions during bloom development not observed during *Varied P* and different from TEP.

480 In order to identify differences between the two series of mesocosm experiments, gel particle
481 abundance was compared to bloom development, which also differed between the experiments.

482 During both experiments, gel particle dynamics were tightly coupled to the production of organic
483 matter during bloom development (Fig. 7, Table 3). Numerical abundances of TEP and CSP were
484 directly related to Chl *a* concentration until the bloom peak (Fig. 7a, d). Thereby, the increase of
485 gel particle abundance with Chl *a* concentration was different for TEP and CSP during *Varied P*
486 as well as during *N*. While TEP abundance increased slightly faster with Chl *a* concentration
487 during *Varied P*, the increase in CSP abundance with Chl *a* concentration was twice as strong
488 during *Varied N* than during *Varied P* (Table 3). After the Chl *a* maxima, gel particle formation
489 continued while Chl *a* concentrations declined, leading to higher [gel particles]:[Chl *a*] ratios
490 towards the end of the experiments (Table 4). Partly decoupled from Chl *a* concentration, gel
491 particles remained tightly coupled to POC and PN dynamics throughout both experiments (Fig.
492 7b, c, e, f). Thereby, a similar coupling was observed between TEP and POC or PN concentration
493 during both experiments, while CSP abundance increased more strongly with POC and PN
494 concentration during *Varied N* (Table 3). The carbon content of TEP (TEP-C) averaged for all
495 mesocosms on day 1 was 0.61 ± 0.29 μmol L^{-1} and 0.72 ± 0.38 μmol L^{-1} for *Varied P* and *Varied*
496 *N*, respectively. During both experiments, TEP-C steadily increased along with the general
497 abundance of TEP. Maximum TEP-C during *Varied P* was reached on day 8 with values of 12.6

– 34.9 µmol L^{-1} representing a share of 31-41 Mol% POC, or 8.4-17.6 Mol% TOC (Table 4). During *Varied N*, final TEP-C concentration contributed with an even higher proportion to the organic carbon pool, equivalent to 22.8-84 Mol % POC or 12-29 Mol % of TOC. Molar ratios of [TEP-C]:[PN] were initially below 1 and increased to averaged 2.2-3.6 during *Varied P* and to 1.8-6.9 during *Varied N*.

A direct coupling was also observed between gel particles and bacterial abundance (Table 3). Like for POC and PN, the relative increase in gel abundance was much steeper during *Varied N* than during *Varied P*, again showing that gel particles in general were more abundant during the second experiment. Although less pronounced than for particulate organic matter, TEP and CSP numerical abundances were also related to DOC concentration during *Varied P* and *Varied N* (Table 3), while no significant relationship was observed between gel particle abundance and DON concentration. In contrast to gel particles, however, DOC was not significantly related to Chl *a* concentration in both experiments, but to POC and PN concentrations (Fig. 7g-i, Table 3). Differences in the relationship of DOC to POC or PN were relatively small, suggesting an only slightly higher increase of DOC with particulates during *Varied N*. DOC concentration correlated significantly with bacterial abundance (Table 3). The increase of DOC concentration relative to bacterial numbers was almost twice as high during *Varied N*, suggesting that bacteria did not catch up with DOC production during the second experiment.

Another comparison of both experiments can be made by relating gel particle abundance to initial [DIN]:[DIP] ratios that covered a similar range during both experiments (Fig. 8). This showed that for similar initial nutrient ratios, maximum abundance of both TEP and CSP were generally

520 higher during the second experiment, *Varied N*. Moreover, only during the second experiment
521 changes in [DIN]:[DIP] ratios had an effect on maximum gel particle abundance.

522 However, direct comparison of the 'centrepoint' treatment 12.0N/0.75P that was realized with 4
523 replicates during *Varied P* and 3 replicates during *Varied N* showed clear differences in organic
524 matter development during the two experiments for mesocosms that received the same nutrient
525 addition (Fig. 9). For this treatment, Chl a concentration, DOC and TEP accumulated about two
526 times more in the course of *Varied N*, while the increase in CSP abundance over time was even
527 threefold higher.

528

529 **4. Discussion**

530 **4.1 Nutrient availability and phytoplankton bloom development**

531 After fertilization with inorganic nutrients, phytoplankton blooms developed in all mesocosms
532 during the two consecutive experiments conducted with natural surface water from the eastern
533 tropical North Atlantic (ETNA). Responses to varied nutrient supply became more obvious after
534 one (or both) macronutrients were exhausted, resulting in a large variation of organic matter
535 concentration among mesocosms and treatments during the bloom peak and post-bloom phases.
536 Accumulation of organic matter during bloom development revealed a generally stronger
537 fertilization effect after addition of different amounts of NO_3^- in the second experiment compared
538 to the first one with varied initial PO_4^{3-} supply. This indicates that biomass production in ETNA
539 surface waters near Cape Verde may be limited by nitrogen rather than by phosphorus
540 availability. However, clear differences between both experiments were also observed for
541 mesocosms receiving the same nutrient supply. This suggests that small differences in the initial

542 conditions of experiments with natural communities, such as during this mesocosm study, can
543 significantly impact the outcome of biogeochemical responses.

544 Moderate variations in responses of planktonic food webs and associated biogeochemical cycling
545 to the same nutrient treatment have been observed previously for mesocosm experiments
546 conducted at different marine ecosystem sites, but a coherent picture of nitrogen stimulation was
547 clearly demonstrated (Olsen et al., 2006; Vadstein et al., 2012).

548 During this study, phytoplankton abundance was lower during the early days of *Varied N*, while
549 bacterial abundance was higher, despite sampling of initial waters at the same location and within
550 a time difference of only a few days. Moreover, differences between *Varied N* and *P* were
551 identified for the initial community composition of diazotrophs (Meyer et al., 2015). We cannot
552 fully exclude that these differences in the initial conditions generally affected the sensitivity to
553 nutrient addition, regardless of the varied nutrient concentration and were also responsible for the
554 higher response in mesocosms where the same nutrient treatment was applied. However, the clear
555 increase in organic matter accumulation with increasing initial NO_3^- concentration is in
556 accordance with previous findings (Franz et al., 2012a) and strongly suggests that ecosystems in
557 the ETNA are controlled by NO_3^- rather than by PO_4^{3-} availability.

558 It should be kept in mind that mesocosm experiments such as conducted during this study can
559 only capture a transient response to perturbation, such as nutrient addition, and mainly give
560 insights to short-term effects on processes. To extrapolate from mesocosm experiments to long--
561 term responses of natural systems is not straightforward. Hence, although the response to NO_3^-
562 addition during the second experiment was pronounced, it represents only one possible outcome.
563 The observed differences for the 12.0N/0.75P treatment indicate that the response of an
564 ecosystem to nutrient supply may vary even in a comparatively stable environment like the

565 ETNA. Clearly, a better knowledge of the impact of ecological variability, e.g. plankton
566 community structure, diversity and acclimation potential, on biogeochemical processes is needed
567 to fully explain differences in the response size to perturbation.

568

569 **4.2 Nutrient effects on gel particle dynamics**

570 Previous studies on TEP and CSP in marine systems have suggested that the rate of gel-particle
571 formation depends on the amount and chemical quality of dissolved precursors (Engel et al.,
572 2004a; Mari and Robert, 2008; Chow et al., 2015). For extracellular organic matter released by
573 bacterio- and phytoplankton, the chemical composition and molecular weight of compounds
574 varies among species, and is also dependent on environmental conditions and physiological status
575 (Aluwihare and Repeta, 1999; Grossart et al., 2007; Borchard and Engel, 2015). Because
576 extracellular release is a major source for gel particle precursors, factors influencing this release
577 likely also affect marine gel particle formation.

578 During this study, a clear accumulation of DOC was observed along with biomass build-up in all
579 mesocosms, indicating that the rate of DOC release exceeded DOC loss processes such as
580 coagulation into gel- particles or microbial uptake and respiration. Higher ΔDOC values were
581 observed shortly after the Chl *a* peak, coinciding with nutrient concentrations being strongly
582 reduced. Enhanced extracellular release of DOC or 'malfunctioning' of the microbial loop, i.e.
583 reduced microbial uptake and respiration of DOC by bacteria, have been suggested to explain
584 DOC accumulation in the ocean, particularly at times when inorganic nutrients become depleted
585 (Myklestad, 1974; Biddanda and Benner, 1997; Thingstad et al., 1997; Engel et al., 2004b).
586 During this study, DOC accumulation was significantly related to the initial NO_3^- concentration
587 during *Varied N*, suggesting a dependence on the trophic status, although no direct relationship to

588 Chl *a* concentration was observed. Higher accumulation of DOC with increasing nitrogen load
589 has been observed during previous mesocosm experiments and explained by a combination of
590 production and recycling of DOC being both higher at higher microbial biomass (Vadstein et al.,
591 2012). In addition, phosphorus limitation may have reduced bacterial utilisation of DOC in
592 mesocosms with high initial [DIN]:[DIP] ratios and below detection levels of PO_4^{3-} after the
593 bloom, when highest accumulation rates of DOC occurred.

594 In contrast to DOC, no accumulation of DON was observed in the course of the experiments in
595 almost all mesocosms, except for the last day of *Varied P* and for those treatments receiving
596 highest NO_3^- additions during *Varied N*. This indicates that loss processes such as microbial
597 utilization of organic nitrogen forms or partitioning of DON into CSP exceeded DON release
598 during this study.

599 In general, little is known about gel particle production at tropical open ocean sites. To the best of
600 our knowledge, this is the first report on TEP and CSP abundance in the ETNA. Data on TEP-C
601 concentration observed during our study (Table 4), however, agree well with observations from
602 Wurl et al. (2011), who determined <2 to 40 µmol C L^{-1} for TEP in surface waters of the Tropical
603 North Pacific(offshore Hawaii).

604 Like DOC, gel-particle abundance during this study was strongly related to the general build-up
605 and decay of autotrophic biomass. Thereby, a significant impact of initial NO_3^- supply on gel
606 particle abundance, especially on CSP, was observed during *Varied N*, as well as a general
607 increase of the maximum abundance of gel particles with the initial [DIN]:[DIP] ratio.

608 An increase of TEP formation, when phytoplankton was grown at higher NO_3^- concentration, is
609 in accordance with earlier observations made during culture and mesocosm experiments (Corzo

et al., 2000; Pedrotti et al., 2010) and has been explained by higher biomass production at higher nutrient loads; a larger biomass leads to a higher amount of released polysaccharides when the autotrophic biomass runs into nutrient limitation. A general relationship between TEP and autotrophic biomass concentration, e.g. determined as Chl *a,* has been observed before (Passow, 2002; Beauvais et al., 2003). Furthermore, species or physiology specific variations in TEP formation by phytoplankton were observed (Berman and Viner-Mozzini, 2001; Claquin et al., 2008; Passow, 2002). During this study, gel particles and Chl *a* dynamics were decoupled after the Chl *a* peak. Hence, despite the general observation that higher autotrophic biomass leads to more gel particles, temporal developments of Chl *a* and gel particle concentration may contrasts between bloom built-up and decay. This is in accordance with earlier studies showing that POC, TEP and CSP concentration continued to increase after the Chl *a* peak (Alldrege, 1995; Engel, 2002; Logan et al., 1994; Mari and Kiørboe, 1996) and can be explained by the 'carbon-overflow' theory (Schartau et al., 2007; Kreus et al., 2015).

During the post-bloom phase, a large proportion of organic carbon was thus channeled to the POC pool in the form of TEP. Carbon contained in TEP, accounted for 0.5 µmol C (initial days) to ~68 µmol C (final days) indicating a much higher DOC production than derived from ΔDOC alone. The ratio of [TEP-C]:[POC] strongly increased during *Varied N,* yielding values of up to 93%. Even though these values are within the range of earlier findings (Engel and Passow, 2001; Pedrotti, 2010), an underestimation of POC, and hence overestimation of [TEP-C]:[POC] ratio, seems likely, because a large proportion of TEP was in the size range 1-2 µm ESD and may not be retained on GF/F filters (nominal pore size 0.7 µm), due to their flexible and non-spherical structure (Engel and Passow, 2001; Pedrotti, 2010). In addition, TEP-C calculation by use of an

empirical relationship to TEP size previously established from phytoplankton cultures could overestimate carbon content of naturally occurring TEP at this site.

A recent study by Rahav et al. (2013) suggested that bacterial diazotrophs in aphotic, DIN-rich layers of the Red Sea and eastern Mediterranean Sea benefit from TEP as organic carbon source, resulting in an increase in aphotic nitrogen fixation with TEP concentration. For the ETNA, unicellular heterotrophic diazotrophs are readily abundant, also below the euphotic zone in high DIN waters (Langlois et al., 2005), and contribute substantially to total nitrogen fixation of the system (Agawin et al., 2014). High TEP production by surface phytoplankton communities in the ETNA as observed during this study, and settling of TEP to aphotic layers, may therefore provide an important labile carbon source for sustaining heterotrophic nitrogen fixation.

While the importance of TEP formation for converting DOC to POC, and related consequences for carbon cycling and export, have been highlighted over the past decades (Alldrege et al., 1995; Passow, 2002; Engel et al., 2004a; Arrigo, 2007), little is known about the role of CSP, on organic carbon and more importantly on organic nitrogen cycling. It is likely that CSP plays a significant role for nitrogen cycling, contributing to DON to PN conversion and to the PN pool as well as providing a nitrogenous resource for auto- and heterotrophic growth. During this study, clearly higher accumulation of CSP relative to Chl *a* was observed during *Varied N*, i.e. when a surplus of inorganic nitrogen was available. As a consequence, CSP contributed more to POC and PON increase during *Varied N* than during *Varied P*. This suggests that higher inorganic nitrogen supply favors production of extracellular PON, which may be subject to bacterial utilization at a later time. Because CSP are proteinaceous particles, their export to depth, e.g. by physical transport or as part of sinking aggregates, may provide important amino acids for microorganisms in aphotic zones, including denitrifying and anammox bacteria. Since labile

amino acids have been suggested to be one important factor limiting organic matter degradation in oxygen minimum zones (Pantoja et al., 2004; 2009), a supply with CSP from the photic zone may also affect total carbon remineralisation and therewith oxygen consumption at deeper depths. Our results furthermore suggest that CSP as proteinaceous particles may include an important fraction of organic nitrogen in the size fraction typically attributed to bacteria.

4.3 Formation, aggregation and degradation of gel particles – Insights from size frequency distributions

Changes in the size frequency distribution of TEP during this study revealed an increase in the proportion of larger particles in the course of phytoplankton blooms, indicating TEP aggregation rather than degradation during both experiments. For CSP, decreasing slopes together with a strong increase in total abundance revealed an increasing number of smaller particles during *Varied N*, indicating new formation of CSP during the phytoplankton bloom and postbloom periods. Occurrence of CSP at the time or depth of the Chl *a* maxima has also been observed during previous studies (Cisternas Novoa et al., 2014; 2015). A clear indication for aggregation processes, i.e. decreasing slopes as for TEP, was not observed for CSP. This is in accordance with findings of Prieto et al. (2002), who suggested that CSP are less involved in aggregate formation during diatom blooms than TEP. CSP number and total area decreased at the end of *Varied N* (day 8), suggesting that loss processes exceeded new CSP formation.

TEP and CSP, both represent hotspots for microbial activity (Azam, 1983; Passow and Alldrege, 1994; Pedrotti, 2009; Grossart, 1998; Bar-Zeev, 2009). However, CSP are per definition proteinaceous particles and thus expected to include high amounts of labile N-compounds. The

observed decrease in CSP abundance at day 8 of *Varied N* can therefore be explained by bacterial degradation in order to liberate N, as suggested earlier (Long and Azam, 1998). Bacteria cell numbers sharply increased from day 5 onwards during both experiments, along with the strongest increase in gel-particle abundance.

5. Conclusion

Gel particles can represent a substantial fraction of organic particles in ETNA ecosystems after nutrient supply, e.g. deep upwelling of water masses. Increasing NO_3^- relative to PO_4^{3-} concentrations favors gel particle formation. Consequently, it may be expected that a reduction of NO_3^- surface water concentrations as a result of increasing ocean anoxia will diminish the abundance of marine gel particles, particularly CSP, with potential implications for aggregation, export and turn-over processes of organic matter in the water column. Particle dynamics of TEP and CSP differ during bloom development; while TEP seem to be more prone to aggregation, potentially enhancing export of organic matter, CSP appear to be a better organic substrate for heterotrophs and may decompose within a few days. Because TEP and CSP are part of the bulk POC and PN pools, changes in the balance of TEP and CSP formation processes such as induced by changes in the $[NO_3^-]$: $[PO_4^{3-}]$ supply ratio will likely impact biogeochemistry during and after phytoplankton blooms as well as food-web dynamics. Biogeochemical responses to variations in nutrient supply and stoichiometry may differ between different pelagic communities, even in supposedly stable ecosystems such as the ETNA.

Acknowledgements

This research was supported by the *Sonderforschungsbereich 754* "Climate-Biogeochemistry Interactions in the Tropical Ocean" (www.sfb754.de), subprojects B2 (J. Meyer), B8 (H. Hauss and R. Kiko) and B9 (A. Engel, C. Borchard, A. Loginova). The *Sonderforschungsbereich 754* is supported by the German Science Foundation (DFG). The authors thank their colleagues from the INDP, Cape Verde, for their assistance with setting up the experiment and acknowledge the support of captain and crew of RV *Islandia* during initial sampling. We furthermore greatly acknowledge the technical support of Jon Roa (DOC, DON) and Ulrike Panknin (nutrients), as well as Nienke Bijma, Clarissa Karthäuser and Sami Manandhar (gel particle microscopy).

References

Agawin, N. S. R., Benavides, M., Busquets, A., Ferriol, P., Stal, L. J., and Aristegui, J.: Dominance of unicellular cyanobacteria in the diazotrophic community in the Atlantic Ocean. Limn. Oceanogr., 59, 2, 623-63, 2014.

Alldredge, A. L., Gotschalk, C., Passow, U., and Riebesell, U.: Mass aggregration of diatom blooms - Insights from a mesocosm study, Deep-Sea Research Part II-Topical Studies in Oceanography, 42, 9-27, 1995.Alldredge, A. L., Passow, U., and Logan, B. E.: The abundance and significance of a class of large, transparent organic particles in the ocean, Deep-Sea Res., 40, 1131-1140, 1993.

Aluwihare, L.I., Repeta, D.J.: A comparison of the chemical characteristics of oceanic DOMand extracellular DOM produced by marine algae, Mar. Ecol.- Prog. Ser., 186, 105-117, 1999.

Arrigo, K. R.: Carbon cycle. Marine manipulations. Nature, 450, 491-492, 2007.

Azam, F., Fenchel, T., Field, J. G., Graf, J. S., Meyer-Rei, L. A., and Thingstad, F.: The ecological role of water- column microbes in the sea. Mar. Ecol. Prog. Ser., 10, 257-263, 1983.

Baines, S. B. and Pace, M. L.: The production of dissolved organic matter by phytoplankton and its importance to bacteria: Patterns across marine and freshwater systems, Limnol. Oceanogr., 36, 1078-1090, 1991.

Baker, A. R., Weston, K., Kelly, S. D., Voss, M., Streu, P., Cape, J. N.: Dry and wet deposition of nutrients from the tropical Atlantic atmosphere: links to primary productivity and nitrogen fixation. Deep-Sea Res., I 54, 10, 1704–1720, 2007.

734 Bar-Zeev, E., Berman-Frank, I., Stambler, N., Vázquez-Domínguez, E., Zohary, T., Capuzzo, E.,
735 Meeder, E., Suggett, D. J., Iluz, D., Dishon, G., and Berman, T.: Transparent exopolymer
736 particles (TEP) link phytoplankton and bacterial production in the Gulf of Aqaba, Aquat.
737 Microb Ecol, 56, 217-225, doi: 10.3354/ame01322, 2009.

738 Beauvais, S., Pedrotti, M. L., Villa, E., and Lemee, R.: Transparent exopolymer particle (TEP)
739 dynamics in relation to trophic and hydrological conditions in the NW Mediterranean Sea,
740 Mar. Ecol. Prog. Ser., 262, 97-109, 2003.

741 Berman, T., and Viner-Mozzini, Y.: Abundance and characteristics of polysaccharide and
742 proteinaceous particles in Lake Kinneret. Aquat. Micr. Ecol., 24, 255-264, 2001.

743 Biddanda, B., and Benner, R.: Carbon, nitrogen, and carbohydrate fluxes during the production of
744 particulate and dissolved organic matter by marine phytoplankton, Limnol. Oceanogr., 42,
745 506-518, 1997.

746 Bjørnsen, P.K.: Phytoplankton exudation of organic matter: Why do healthy cells do it?, Limnol.
747 Oceanogr., 33, 151-154, 1988.

748 Borchard,C., Borges, A., Händel, N. and Engel, A. Biogeochemical response of *Emiliania*
749 *huxleyi* (PML B92/11) to elevated CO_2 and temperature under phosphorous limitation: a
750 chemostat study. Journal of Experimental Marine Biology and Ecology, 410 . pp. 61-71,
751 2011.

752 Borchard, C., and Engel, A.: Organic matter exudation by *Emiliania huxleyi* under simulated
753 future ocean conditions Biogeosciences (BG), 9 (8). pp. 3405-3423. DOI 10.5194/bg-9-
754 3405-2012, 2012.

Borchard, C. and Engel, A.: Size-fractionated dissolved primary production and carbohydrate composition of the coccolithophore *Emiliania huxleyi,* Biogeosciences, 12, 1271-1284, 2015.

Chin, W.C., Orellana, M.V., and Verdugo, P.: Spontaneous assembly of marine dissolved organic matter into polymer gels, Nature, 391, 568-572, 1998.

Chow, J. S., Lee, C., and Engel, A.: The influence of extracellular polysaccharides, growth rate, and free coccoliths on the coagulation efficiency of *Emiliania huxleyi*. Mar. Chem., 175, 5-15, 2015.

Cisternas-Novoa, C., Lee, C., and Engel, A.: A semi-quantitative spectrophotometric, dye-binding assay for determination of Coomassie Blue stainable particles. Limnol. Oceanogr. Methods, 12, 604-616, 2014.

Cisternas-Novoa, C., Lee, C., and Engel, A.: Transparent exopolymer particles (TEP) and Coomassie stainable particles (CSP): Differences between their origin and vertical distributions in the ocean. Mar. Chem., 175, 56-71, 2015.

Claquin, P., Probert, I., Lefebvre, S., and Veron, B.: Effects of temperature on photosynthetic parameters and TEP production in eight species of marine microalgae. Aquat. Micr. Ecol. 51, 1-11, 2008.

Corzo, A; Morillo, JA; and Rodriguez, S.: Production of transparent exopolymer particles (TEP) in cultures of *Chaetoceros calcitrans* under nitrogen limitation, Aquatic Microb. Ecol., 23, 1, 63-72, 2000.

Del Giorgio, P. A. and Duarte, C.: Respiration in the open ocean. Nature, 420, 379-384, 2002.

776 Deutsch, C., Sarmiento, J. L., Sigman, D. M., Gruber, N., and Dunne, J. P.: Spatial coupling of
777 nitrogen inputs and losses in the ocean, Nature, 445, 7124, 163-167, 2007.

778 Ducklow H.W., Purdie D.A., Williams P.J.L., and Davies J.M.: Bacterioplankton - a sink for
779 carbon in a coastal marine plankton community, Science, 232, 865-867, 1986.

780 Engel, A., and Passow, U.: Carbon and nitrogen content of transparent exopolymer particles
781 (TEP) in relation to their Alcian Blue adsorption, Mar Ecol-Prog Series, 219, 1-10, 2001.

782 Engel, A.: Direct relationship between CO_2 uptake and transparent exopolymer particles
783 production in natural phytoplankton, J. Plankton Res., 24, 49-53, 2002.

784 Engel, A., Thoms, S., Riebesell, U., Rochelle-Newall, E. and Zondervan, I.: Polysaccharide
785 aggregation as a potential sink of marine dissolved organic carbon, Nature, 428 , 929-932,
786 2004a.

787 Engel, A., Delille, B., Jacquet, S., Riebesell, U., Rochelle-Newall, E., Terbrüggen, A. and
788 Zondervan, I.: Transparent exopolymer particles and dissolved organic carbon production
789 by *Emiliania huxleyi* exposed to different CO_2 concentrations: a mesocosm experiment,
790 Aquat. Microb. Ecol., 34, 93-104, 2004b.

791 Engel, A.: Determination of Marine Gel Particles, Practical Guidelines for the Analysis of
792 Seawater. CRC Press. 2009.

793 Engel, A., Händel, N., Wohlers, J., Lunau, M., Grossart, H. P., Sommer, U. uand Riebesell, U.:
794 Effects of sea surface warming on the production and composition of dissolved organic
795 matter during phytoplankton blooms: results from a mesocosm study, Journal of Plankton
796 Research, 33, 3, 357-372, 2011.

797 Engel, A., Piontek, J., Grossart, H. P., Riebesell, U., Schulz, K. G. and Sperling, M.: Impact of
798 CO2 enrichment on organic matter dynamics during nutrient induced coastal
799 phytoplankton blooms, Journal of Plankton Research, 36, 641-657, 2014.

800 Falkowski, P. G.: Rationalizing elemental ratios in unicellular algae. J. Phycol., 36: 3-6, 2000.

801 Fogg, G. E.: The ecological significance of extracellular products of phytoplankton
802 photosynthesis, Bot. Mar., 26, 3-14, 1983.

803 Fraga, F. Phytoplanktonic biomass synthesis: application to deviations from Redfield
804 stoichiometry, Sci. Mar., 65, 153-169, 2001.

805 Franz, J. M. S., Hauss, H., Sommer, U., Dittmar, T., and Riebesell, U: Production, partitioning
806 and stoichiometry of organic matter under variable nutrient supply during mesocosm
807 experiments in the tropical Pacific and Atlantic Ocean. Biogeosciences, 9, 4629-4643,
808 doi:10.5194/bg-9-4629-2012, 2012a.

809 Franz, J., Krahmann, G., Lavik, G., Grasse, P., Dittmar, T., and Riebesell, U.: Dynamics and
810 stoichiometry of nutrients and phytoplankton in waters influenced by the oxygen
811 minimum zone in the eastern tropical Pacific, Deep-Sea Res. Part I, 62, 20-31, 2012b.

812 Galgani, L., Stolle, C., Endres, S., Schulz, K. G. and Engel, A.: Effects of ocean acidification on
813 the biogenic composition of the sea-surface microlayer: Results from a mesocosm study.
814 Journal of Geophysical Research - Oceans, 119, 7911-7924. DOI 10.1002/2014JC010188,
815 2014

816 Geider, R. J. and LaRoche, J.: Redfield revisited: variability of C:N:P in marine microalgae and
817 its biochemical basis, Eur. J. Phycol., 37, 1-17, 2002.

818 Goldman, J. C., McCarthy, J. J., and Peavey, D. G.: Growth rate influence on the chemical
819 composition of phytoplankton in oceanic waters, Nature, 279, 210-215, 1979.

820 Grasshoff, K., Kremling K., and Ehrhardt M.: Methods of seawater analysis, 3rd ed. Wiley1999.

821 Grossart, H.P., Berman, T., Simon, M., and Pohlmann, K.: Occurrence and microbial dynamics
822 of macroscopic organic aggregates (lake snow) in Lake Kinneret, Israel, in fall, Aquat.
823 Microb. Ecol., 14, 59-67, 1998.

824 Grossart, H., Engel, A., Arnosti, C., De La Rocha, C. L., Murray, A. E., and Passow, U.:
825 Microbial dynamics in autotrophic and heterotrophic seawater mesocosms. III. Organic
826 matter fluxes, Aquat. Microb. Ecol. , 49, 143-156, 2007.

827 Gruber, N., and Sarmiento, J. L.: Global patterns of marine nitrogen fixation and denitrification,

828 Hansell, D. A., Bates, N. R., and Olson, D. B.: Excess nitrate and nitrogen fixation in the North
829 Atlantic Ocean. Mar. Chem., 84, 3–4, 243–265, 2004.

830 Hauss, H., Franz, J. M. S., Hansen, T., Struck, U. and Sommer U.: Relative inputs of upwelled
831 and atmospheric nitrogen to the eastern tropical North Atlantic food web: Spatial
832 distribution of $\delta^{15}N$ in meso zooplankton and relation to dissolved nutrient dynamics.
833 Deep-Sea Research I 75: 135–145, 2013. doi: 10.1016/j.dsr.2013.01.010

834 Hauss, H., Franz, J. M. S. and Sommer U.: Changes in N:P stoichiometry influence taxonomic
835 composition and nutritional quality of phytoplanton in the Peruvian Upwelling. Journal of
836 Sea Research 73: 74-85, 2012. doi: 10.1016/j.seares.2012.06.010

837 Karstensen, J., Fiedler, B., Schütte, F., Brandt, P., Körtzinger, A., Fischer, G., Zantopp, R., Hahn,
838 J., Visbeck, M., and Wallace, D.: Open ocean dead-zone in the tropical North Atlantic
839 Ocean, Biogeosciences Discuss., 11, 17391-17411, doi:10.5194/bgd-11-17391-2014,
840 2014.

841 Klausmeier, C. A., Litchman, E., Daufresne, T., and Levin, S. A.: Optimal nitrogen-to-
842 phosphorus stoichiometry of phytoplankton, Nature, 429, 171-174, 2004.

843 Kreus, M., Schartau, M., Engel, A., Nausch, M. and Voss, M.: Variations in the elemental ratio
844 of organic matter in the central Baltic Sea: Part I—Linking primary production to
845 remineralization Continental Shelf Research, 100, 25-45, 2015. DOI
846 10.1016/j.csr.2014.06.015.

847 Kuypers, M. M. M., Lavik, G., Woebken, D., Schmid, M., Fuchs, B. M., Amann, R., Jørgensen,
848 B. B., and Jetten, M. S. M.: Massive nitrogen loss from the Benguela upwelling system
849 through anaerobic ammonium oxidation. Proc. Natl. Acad. Sci. 102, 6478–6483, doi:
850 10.1073/pnas.0502088102, 2005.

851 Lam, P., and Kuypers, M. M. M: Microbial Nitrogen Cycling Processes in Oxygen Minimum
852 Zones. Annu. Rev. Mar. Sci., 3, 317–45, 2011.
853
854 Langlois, R. J., LaRoche, J., and Raab, P. A.: Diazotrophic Diversity and Distribution in the
855 Tropical and Subtropical Atlantic Ocean, Appl. Environ. Microbiol., 71, 7910-7919,
856 2005.

857 Logan, B. E., Grossart, H.-P., and Simon, M.: Direct observation of phytoplankton, TEP and
858 aggregates on polycarbonate filters using brightfield microscopy, J. Plankt. Res., 16,
859 1811-1815, 1994.

860 Long, R.A., and Azam, F.: Abundant protein-containing particles in the sea, Aquat. Microb.
861 Ecol., 10, 213-221, 1996.

862 Mague, T.H., Friberg, E., Hughes, D.J., and Morris, I.: Extracellular release of carbon by marine
863 phytoplankton; a physiological approach, Limnol. Oceanogr. 25, 262-279, 1980.

864 Mari, X., and Kiørboe T.: Abundance, size distribution and bacterial colonization of transparent
865 exopolymeric particles (TEP) during spring in the Kattegat, J. Plankton Res., 18, 969-986,
866 doi: 10.1093/plankt/18.6.969, 1996.

867 Mari, X., and Robert, M.: Metal induced variations of TEP sticking properties in the
868 southwestern lagoon of New Caledonia. Mar. Chem., 110, 98–108, 2008.

869
870 Mari, X.: Carbon content and C:N ratio of transparent exopolymeric particles (TEP) produced by
871 bubbling exudates of diatoms. Mar. Ecol. Progr. Ser., 183, 59-71, 1999.

872 Meyer, J., Löscher, C. R., Neulinger, S. C., Reichel, A. F., Loginova, A., Borchard, C., Schmitz,
873 R. A., Hauss, H., Kiko, R. and U. Riebesell: Changing nutrient stoichiometry affects
874 phytoplankton production, DOP build up and dinitrogen fixation – a mesocosm
875 experiment in the eastern tropical North Atlantic. Biogeosciences Discuss., 12, 9991-
876 10029, 2015.

877 Mills, M.M., and Arrigo, K.R.: Magnitude of oceanic nitrogen fixation influenced by the nutrient
878 uptake ratio of phytoplankton, Nature Geoscience, 3, 412-416, 2010.

879 Myklestad, S.: Production of carbohydrates by marine planktonic diatoms I, Comparison of nine
880 different species in culture, J. Exp. Mar. Biol. Ecol., 15, 261-274, 1974.

881 Nagata, T.: Production mechanisms of dissolved matter. In Kirchmann, D. L. (ed.), Microbial
882 Ecology of the Oceans, First edition, Wiley-Liss, New York, 121-152, 2000.

883 Olsen, Y., Agusti, S., Andersen, T., Duarte, C. M. , Gasol, J. M. , Gismervik, I. , Heiskanen, A-
884 S., Hoell, E., Kuuppo, P. , Lignell, R., Reinertsen, H., Sommer, U., Stibor, H., Tamminen,
885 T., Vadstein, O., Vaque, D., Vidal, M.: A comparative study of responses in planktonic
886 food web structure and function in contrasting European coastal waters exposed to
887 experimental nutrient addition, Limn. Oceanogr., 51, 1, 488-503, 2006.

888 Pantoja, S., Sepulveda, J. S., and Gonzalez, H. E.: Decomposition of sinking proteinaceous
889 material during fall in the oxygen minimum zone off northern Chile, Deep-Sea Research
890 Part I-Oceanographic Research Papers, 51, 55-70, 10.1016/j.dsr.2003.09.005, 2004.

891 Pantoja, S., Rossel, P., Castro, R., Cuevas, L. A., Daneri, G., and Cordova, C.: Microbial
892 degradation rates of small peptides and amino acids in the oxygen minimum zone of
893 Chilean coastal waters, Deep-Sea Research Part Ii-Topical Studies in Oceanography, 56,
894 1019-1026, 10.1016/j.dsr2.2008.09.007, 2009.

895 Parsons, T.R., Maita, Y., and Lalli, C.M.: A manual of chemical and biological methods for
896 seawater analysis Pergamon Press Oxford, UK, 173pp, 1984.

897 Passow, U., Shipe, R. F., Murray, A., Pak, D. K., Brzezinski, M. A., and Alldredge, A. L.: The
898 origin of transparent exopolymer particles (TEP) and their role in the sedimentation of
899 particulate matter. Cont. Shelf Res., 21, 4 , 327-346, 2001.

900 Passow, U.: Transparent exopolymer particles (TEP) in aquatic environments. Prog. Oceanogr.
901 55, 3-4, 287-333, 2002.

902 Pedrotti, M. L., Peters, F., Beauvais, S., Vidal, M., Egge, J., Jacobsen, A., Marrase, C.: Effects of
903 nutrients and turbulence on the production of transparent exopolymer particles: a
904 mesocosm study, Mar. Ecol. Prog. Ser., 419, 57-69, 2010.

905 Prieto, L., Ruiz, J., Echevarría, F., García, C. M., Bartual, A., Gálvez, J. A., Corzo, A., and D.
906 Macías: Scales and processes in the aggregation of diatom blooms: high time resolution
907 and wide size range records in a mesocosm study. Deep Sea Res. Part I 49(7), 1233-1253,
908 2002.

909 Radic, T., Ivancic, I., Fuks, D., and Radic, J. Marine bacterioplankton production of
910 polysaccharidic and proteinaceous particles under different nutrient regimes. FEMS
911 Microb. Ecol., 58 , 3, 333-342, 2006.

912 Rahav, E., Bar-Zeev, E., Ohayon, S., Elifantz, H., Belkin, N., Herut, B., Mulholland, M. R., and
913 Berman-Frank, I.: Dinitrogen fixation in aphotic oxygenated marine environments.
914 Frontiers in Mar. Microbiol., 4, 227, 1-11, 2013.

915 Redfield, A. C.: The biological control of chemical factors in the environment. Am. Sci., 46, 205-
916 221, 1958.

917 Redfield, A. C., Ketchum, B. H., and Richards, F. A.: The influence of organisms on the
918 composition of seawater. In: The sea, ideas and observations on progress in the study of
919 the seas, Vol 2, M. N. Hill (editor), Interscience, 26-77, 1963.

920 Rhee, G. Y.: Effect of N:P atomic ratios and nitrate limitation on algal growth, cell composition,
921 and nitrate uptake. Limnol. Oceanogr., 23, 10-25, 1978.

922 Sarmiento, H., and Gruber, N. L.: Global patterns of marine nitrogen fixation and denitrification.
923 Global Biogeochem. Cycles, 11(2), 235-266, 1997

924 Schartau, M., Engel, A., Schröter, J., Thoms, S., Völker, C., and Wolf-Gladrow, D.: Modelling
925 carbon overconsumption and the formation of extracellular particulate organic carbon,
926 Biogeosciences, 4, 433-454, 2007.

927 Schneider, B., Engel, A. and Schlitzer, R.: Effects of depth- and CO2-dependent C:N ratios of
928 particulate organic matter (POM) on the marine carbon cycle, Global Biogeochemical
929 Cycles, 18 (2), 1-13. DOI 10.1029/2003GB002184, 2004.

930 Sharp, J. H.: Improved analysis for particulate organic carbon and nitrogen from seawater
931 Limnol.Oceanogr., 19, 984-989, 1974.

932 Sharp, J. H.: Excretion of organic matter by marine phytoplankton - Do healthy cells do it?
933 Limnol. Oceanogr., 22, 381-399, 1977.

934 Sommer, U; Hansen, T; Stibor, H; and Vadstein, O.: Persistence of phytoplankton responses to
935 different Si : N ratios under mesozooplankton grazing pressure: a mesocosm study with
936 NE Atlantic plankton. Mar. Ecol. Prog. Ser., 278, 67-75, 2004.

937 Sterner, R. W., and Elser, J. J.: Ecological Stoichiometry: The Biology of Elements from
938 Molecules to the Biosphere ISBN: 9780691074917 464 pp. 2002

939 Stramma, L., Johnson, G. C., Sprintall, J., and Mohrholz, V.: Expanding Oxygen-Minimum
940 Zones in the Tropical Oceans, Science, 320, 655-658, doi: 10.1126/science.1153847,
941 2008.

Sugimura, Y., and Suzuki, Y.: A high-temperature catalytic oxidation method for the determination of non-volatile dissolved organic carbon in seawater by direct injection of a liquid sample, Mar. Chem., 24, 2, 105–131, 1988.

Thingstad, T. F., Hagstrom, A., and Rassoulzadegan, F.: Accumulation of degradable DOC in surface waters: Is it caused by a malfunctioning microbial loop?, Limnology and Oceanography, 42, 398-404, 1997.

Thornton, D. C. O.: Effect of low pH on carbohydrate production by a 1815 marine planktonic diatom (Chaetoceros muelleri), Research Letters in Ecology, Article ID 105901, 2009.

Toggweiler, J. R.: Carbon overconsumption, Nature, 363, 210-211, 1993.

Vadstein, O., Andersen, T., Reinertsen, H. R., and Olsen, Y.: Carbon, nitrogen and phosphorus resource supply and utilisation for coastal planktonic heterotrophic bacteria in a gradient of nutrient loading. Mar. Ecol. Prog. Ser., 447, 55-75, 2012.

Verdugo, P., Alldredge, A. L., Azam, F., Kirchman, D. L., Passow, U., and Santschi, P. H.: The oceanic gel phase: a bridge in the DOM-POM continuum. Mar. Chem. 92, 67-85, 2004.

Wood, M.A., van Valen, L. M.: Paradox lost? On the release of energy-rich compounds by phytoplankton, Marine Microbial Food Webs 4, 103-116, 1990.

Wurl, O., L. Miller, and Vagle, S. Production and fate of transparent exopolymer particles in the ocean, J. Geophys. Res., 116, C00H13, doi:10.1029/2011JC007342, 2011.

Tables

Table 1: Summary of initial conditions of the seawater used to fill the mesocosms during the two experiments, target nutrient concentrations (Treat-ID), and different nutrient conditions inside the mesocosms after nutrient addition (day 1).

			Varied P					***Varied N***	
Day 0									
Latitude			16.74°N					16.76°N	
Longitude			25.16°W					25.16°W	
POC [µmol L^{-1}]			13.6 ± 3.8					11.9 ± 1.9	
PON [µmol L^{-1}]			1.85 ± 0.68					1.54 ± 0.26	
POP [µmol L^{-1}]			0.10 ± 0.02					0.07 ± 0.01	
Chl *a* [µg L^{-1}]			0.38 ± 0.09					0.18 ± 0.05	
DOC [µmol L^{-1}]			95 ± 4.6					96± 3.9	
DON [µmol L^{-1}]			8.8 ± 1.1					11 ± 1.5	
Day 1									
Mesocosm	Nitrate [µmol L^{-1}]	Phosphate [µmol L^{-1}]	DIN:DIP	Treat - ID		Mesocosm	Nitrate [µmol L^{-1}]	Phosphate [µmol L^{-1}]	DIN:DIP	Treat - ID
MK 13	11.2	0.15	76.8	12.0N/0.25P		MK 13	2.1	0.46	4.5	2.0N/0.75P
MK 14	11.2	0.16	69.8	12.0N/0.25P		MK 15	1.9	0.56	3.3	2.0N/0.75P
MK 16	11.3	0.15	75.8	12.0N/0.25P		MK 16	2.7	0.48	5.6	2.0N/0.75P
MK 1	11.5	0.73	15.8	12.0N/0.75P		MK 9	4.6	0.45	10.4	4.0N/0.75P
MK 2	11.0	0.68	16.1	12.0N/0.75P		MK 11	4.5	0.47	9.6	4.0N/0.75P
MK 3	10.6	0.52	20.5	12.0N/0.75P		MK 12	4.0	0.49	8.2	4.0N/0.75P
MK 10	10.8	0.61	17.6	12.0N/0.75P		MK 14	12.6	0.47	27.0	12.0N/0.75P
MK 6	10.7	1.14	9.4	12.0N/1.25P		MK 4	12.4	0.51	24.3	12.0N/0.75P
MK 7	11.2	1.12	9.9	12.0N/1.25P		MK 1	12.6	0.51	24.7	12.0N/0.75P
MK 8	10.9	1.09	10.0	12.0N/1.25P		MK 2	20.6	0.47	43.9	20.0N/0.75P
MK 9	10.5	1.57	6.7	12.0N/1.75P		MK 3	20.6	0.45	45.9	20.0N/0.75P
MK 11	10.8	1.58	6.9	12.0N/1.75P		MK 6	21.9	0.45	48.8	20.0N/0.75P
MK 12	11.1	1.53	7.2	12.0N/1.75P		MK 7	6.7	0.78	8.5	6.0N/1.03P
MK 4	5.7	1.00	5.7	6.35N/1.10P		MK 8	6.9	0.18	39.4	6.35N/0.40P
MK 15	16.9	1.01	16.7	17.65N/1.10P		MK 10	18.5	0.22	84.3	17.65N/0.40P
						MK 5	18.4	0.79	23.4	17.65N/1.10P
Legends	✶	12.0N/0.25P					×	2.00N/0.75P		
	●	12.0N/0.75P					○	4.00N/0.75P		
	▽	5.35N/1.10P					▽	6.00N/1.10P		
	■	17.65N/1.10P					◆	6.35N/0.40P		
	×	12.0N/1.25P					●	12.0N/0.75P		
	△	12.0N/1.75P					✶	17.65N/0.40P		
							■	17.65N/1.10P		
							♀	20.0N/0.75P		

Table 2: Mean deviations (MD) from the average development, averaged for each mesocosm for the full experimental period (day 1-day8) and Pearson coefficients for correlations of MD versus initial nutrient concentration [µmol L^{-1}]; bold numbers indicate significant correlation (p<0.05).

Varied P	Chl*a*	Bact	POC	PN	DOC	DON	TEP	CSP	*Varied N*	Chla	Bact	POC	PN	DOC	DON	TEP	CSP
treatment	μL^{-1}	$10^5 L^{-1}$	µM	µM	µM	µM	$10^6 L^{-1}$	$10^5 L^{-1}$	treatment	μL^{-1}	$10^5 L^{-1}$	µM	µM	µM	µM	$10^6 L^{-1}$	$10^5 L^{-1}$
12.0N/0.75P	-0.21	2.84	2.45	0.35	3.81	-0.27	4.42	2.07	12.0N/0.75P	0.15	-1.70	4.24	0.61	3.3	1.1	-6.47	-4.23
12.0N/0.75P	0.03	-0.65	1.93	0.14	-1.39	-0.54	21.16	3.32	12.0N/0.75P	0.23	1.12	4.87	0.56	2.7	-0.6	1.78	14.98
12.0N/0.75P	0.06	-0.69	3.35	0.71	-0.74	0.00	16.00	4.73	12.0N/0.75P	0.64	1.10	11.32	1.34	-0.7	-0.9	5.09	12.60
12.0N/0.75P	0.06	3.61	-0.10	0.29	-4.41	0.19	0.53	-5.63	-	-	-	-	-	-	-	-	-
17.65N/1.10P	0.54	4.14	4.07	0.83	3.15	-0.38	7.77	5.48	17.65N/1.10P	0.76	4.24	2.34	0.75	-1.4	-0.5	-7.40	8.06
12.0N/0.25P	-0.28	-1.44	-8.30	-1.14	-4.86	0.49	-19.47	3.39	2.00N/0.75P	-1.01	-1.58	-4.51	-1.14	-2.3	-0.5	-15.10	-18.80
12.0N/0.25P	-0.26	-0.46	-6.51	-0.99	-4.39	0.56	-17.77	-6.21	2.00N/0.75P	-1.04	-1.89	-14.10	-2.12	-9.3	3.4	-21.78	-19.77
12.0N/0.25P	-0.30	-1.09	-2.00	-0.67	-0.10	0.13	-17.16	-4.46	2.00N/0.75P	1.05	1.85	7.29	1.51	1.5	-0.1	17.43	-1.03
6.35N/1.10P	-0.29	-0.79	-0.47	-0.35	-2.48	-0.51	5.83	-4.87	4.00N/0.75P	-0.62	-0.52	-5.46	-1.05	-3.9	-0.7	1.07	-9.07
12.0N/1.25P	0.03	0.28	4.86	0.58	2.84	-0.41	0.59	0.15	4.00N/0.75P	0.91	-0.79	7.45	1.17	6.2	-0.3	15.35	16.30
12.0N/1.25P	0.16	-0.73	0.39	0.10	5.46	0.24	10.52	-2.35	4.00N/0.75P	-0.22	-0.79	-6.56	-1.54	-2.4	-1.6	3.12	-9.56
12.0N/1.25P	0.38	-1.32	2.71	0.19	4.69	0.06	6.48	-6.93	6.00N/1.03P	-0.65	-2.14	-12.28	-1.73	-0.1	-1.3	-23.60	-8.95
12.0N/1.75P	0.13	-2.16	-1.61	-0.40	-2.89	0.04	3.00	4.16	6.35N/0.40P	-1.09	-2.20	-8.85	-1.38	-18.8	-2.2	-15.68	-14.42
12.0N/1.75P	-0.27	-0.83	-4.35	-0.19	4.07	-0.12	-15.74	4.07	17.65N/0.40P	1.31	1.30	14.47	2.76	4.2	0.8	33.98	24.11
12.0N/1.75P	0.23	-0.70	1.66	0.26	-2.75	0.51	-6.15	3.07	20.0N/0.75P	-0.49	1.26	0.10	-0.25	0.5	0.1	-5.21	-0.84
									20.0N/0.75P	-0.88	-0.88	-10.83	-1.58	-4.8	0.3	-21.95	-9.19
									20.0N/0.75P	0.94	1.62	10.52	2.08	7.7	1.8	39.38	19.81
$r(PO_4^{3-})$ =	**0.45**	-0.10	0.37	0.41	0.39	-0.24	0.25	0.31	$r\ (NO_3^-)$=	**0.97**	**0.70**	**0.87**	**0.94**	**0.71**	0.18	**0.80**	**0.86**

Table 3: Statistics for linear regression analysis of gel particle numerical abundance and DOC concentration against organic matter components during mesocosm experiments with different initial PO_4^{3-} (*Varied P;* µmol L^{-1}) and NO_3^- (*Varied N;* µmol L^{-1}) concentrations. Units TEP: x10^7 L^{-1}, CSP: x10^6 L^{-1}, POC: µmol L^{-1}, PN: µmol L^{-1}, Chl *a* : µg L^{-1}, DOC µmol L^{-1}, bacteria x10^6 mL^{-1} , *a* is the slope and *b* is the intercept. See figure 7 for further information.

	Varied P				***Varied N***			
	a	*b*	n	r^2	*a*	*b*	n	r^2
TEP vs.								
Chla	2.0±0.22	1.27±0.39	60	0.65	1.2±0.08	1.52±0.26	96	0.69
POC	0.18±0.012	-0.63±0.49	89	0.72	0.22±0.13	-1.5±0.60	128	0.70
PN	1.2±0.07	-1.4±0.4	89	0.80	1.5±0.1	-1.2±0.7	128	0.64
DOC	0.14±0.02	-8.7±2.2	90	0.34	0.22±0.02	-18±2.1	127	0.54
bacteria	3.4±0.4	0.78±0.67	90	0.46	6.8±0.9	-1.3±1.1	128	0.32
CSP vs.								
Chla	1.3±0.1	1.4±0.3	60	0.76	2.5±0.15	3.2±0.5	96	0.74
POC	0.11±0.01	0.3±0.4	89	0.58	0.25±0.01	-1.2±0.6	112	0.77
PN	0.7±0.06	0.2±0.3	89	0.65	1.9±0.09	-0.1±0.6	112	0.80
DOC	0.10±0.01	-6.6±1.4	90	0.42	0.21±0.03	-13±3.0	111	0.35
bacteria	2.3±0.26	0.63±0.43	90	0.49	8.8±0.84	-2.3±1.11	128	0.47
DOC vs.								
Chla	*n.s*	-	-	-	*n.s.*	-	-	-
POC	0.54±0.06	88±2	119	0.38	0.66±0.05	88±2	127	0.58
PN	3.5±0.4	88±2	119	0.38	4,2±0.4	90±3	127	0.47
bacteria	11±1.5	92±2	119	0.31	21±3.1	88±4	127	0.27

Table 4: Ratios of estimated carbon content of transparent exopolymer particles (TEP-C) to concentrations of particulate organic carbon (POC), total organic carbon (TOC), particulate nitrogen (PN) and Chl *a*. Average values (mean for TEP-C, median for ratios) are given for replicate treatments on day 1 and 8 during *Varied P* and *Varied N*, respectively.

Sampling	*n*	Treat_ID	TEP-C [µmol L^{-1}]	TEP-C : POC [mol %]	TEP-C : TOC [mol %]	TEP-C : PN [mol:mol]	TEP-C : Chl *a* [µM:µg L^{-1}]
Varied P							
Day 1	3	12.0N/0.25P	0.52	3.01	0.48	16.3	0.25
1	4	12.0N/0.75P	0.40	3.12	0.36	3.4	0.26
1	1	6.35N/1.10P	0.98	5.98	0.83	13.0	0.45
1	1	17.65N/1.10P	0.52	4.14	0.45	7.5	0.28
1	3	12.0N/1.25P	0.49	3.99	0.46	4.7	0.29
1	3	12.0N/1.75P	0.55	5.12	0.50	4.4	0.38
Day 8	3	12.0N/0.25P	13	41	8.4	2.21	25
8	4	12.0N/0.75P	16	15	10.4	2.62	28
8	1	6.35N/1.10P	21	28	14.8	2.85	63
8	1	17.65N/1.10P	22	31	13.3	2.77	61
8	3	12.0N/1.25P	18	26	9.9	2.79	32
8	3	12.0N/1.75P	35	19	17.6	3.63	83
Varied N							
Day 1	3	2.0N/0.75P	0.36	3.07	0.29	0.21	2.04
1	3	4.0N/0.75P	0.62	4.90	0.54	0.36	3.84
1	1	6.0N/1.03P	0.50	4.99	0.48	0.41	4.18
1	1	6.35N/0.40P	0.51	4.56	0.47	0.35	3.63
1	3	12.0N/0.75P	0.88	7.34	0.90	0.66	5.16
1	1	17.65N/0.40P	1.77	14	1.67	1.12	9.33
1	1	17.65N/1.10P	0.97	9.32	0.91	0.66	7.43
1	3	20.0N/0.75P	0.75	4.86	0.68	0.40	4.37
Day 8	3	2.0N/0.75P	25	52	12.0	3.42	47
8	3	4.0N/0.75P	46	82	22.4	6.61	48
8	1	6.0N/1.03P	35	87	18.9	6.88	36
8	1	6.35N/0.40P	37	53	17.3	4.03	45
8	3	12.0N/0.75P	40	43	15.6	3.51	43
8	1	17.65N/0.40P	68	93	29.1	6.36	81
8	1	17.65N/1.10P	23	26	9.7	1.79	14
8	3	20.0N/0.75P	42	47	16.1	3.16	19

Figure captions:

Fig. 1, a-f: Bloom development during two series of mesocosms experiments with varied supply of PO_4^{3-} (*Varied P;* a, c, e; *n*=16) or NO_3^- (*Varied N;* b, d, f*; n*=16), respectively. Shaded areas indicate the range (min-max) of data observed during both treatments for Chl *a* concentration (a, b), bacterial abundance (c, d) and particulate organic carbon (POC) concentration (e, f).

Fig. 2, a-d: Nutrient concentrations during two series of mesocosm experiments with varied supply of PO_4^{3-} (*Varied P;* a, c; *n*=16) or NO_3^- (*Varied N;* b, d; *n*=16), respectively. For treatments with identical nutrient supply, average values are given ±1 standard deviation (error bars). See table 1 for explanation of symbols.

Fig. 3, a-d: Changes in dissolved organic carbon (ΔDOC; a, b) and dissolved organic nitrogen (ΔDON; c, d) concentration during *Varied P* (a, c) and *Varied N* (b, d). Values are given as difference to day 1. For treatments with identical nutrient supply, average values are given ±1 standard deviation (error bars). The dashed line visualizes the zero value; symbols as in Table 1.

Fig. 4, a-d: Temporal changes in the total numerical abundance of transparent exopolymer particles (TEP; a, b) and of Coomassie stainable particles (CSP; c, d) during *Varied P* (a, c) and *Varied N* (b, d). For treatments with identical nutrient supply, average values are given ±1 standard deviation (error bars). The dashed line visualizes the zero value; symbols as in Table. 1.

Fig. 5, a-d: Size frequency distribution of gel particles. Calculation of the size frequency distribution slope exemplified for TEP, averaged for all mesocoms on day 1 (circles) and 8 (triangles) during *Varied P* (a) and *Varied N* (b), respectively and for CSP on day 2 (circles) and

8 (triangles) during *Varied P* (c) and *Varied N* (d). Linear regression of log[$dN/d(d_p)$] versus log[d_p] was fitted to the particles in the size range of 1.05 – 14.14 µm ESD (solid symbols).

Fig. 6, a-d: Changes in the slope (δ) of the size frequency distribution of TEP (a, b) and CSP (c, d) during the mesocosm blooms. The grey lines indicate the mean value of all mesocosms on the respective day; symbols as in Table 1.

Fig. 7, a-i: Relationships between organic components during *Varied P* and *Varied N*. Solid symbols: data obtained during *Varied P;* open symbols: data obtained during *Varied N*. Linear regressions with Chl *a* include data of samplings 1, 2 and 5 for *Varied P* and 1-6 for *Varied N*. Linear regressions with POC and PN include data of all samplings. Information on regression statistics is given in table 2.

Fig. 8, a-b: The maximum numerical abundance of TEP (a) and CSP (b) in the mesocosms increased with the initial (day 1) [DIN]:[DIP] ratio during *Varied N* (open symbols), but not during *Varied P* (solid symbols).

Fig 9, a-c: Comparison of Chl *a* concentration (a), accumulation of DOC (b, open symbols) and DON (b, solid symbols), and abundance of TEP (c, open symbols) and CSP (c, solid symbols) observed in the course of the two mesocosms experiments for the treatment 12.0N/0.75P. Direct relationships ([$y_{Varied\ N}$] = a [$x_{Varied\ P}$]+b) were observed for Chl *a,* with a=2.3±0.2, r^2=0.94, n=8; DOC with a=2.1±0.4, r^2=0.84, n=8, TEP with a= 1.7±0.4, r^2=0.78, n=6 and CSP with a=3.3±0.7, r^2=0.86, n=6. Symbols represent mean values of 3 mesocosms (*Varied P*) or 4 mesocosms (*Varied N*) with ± 1 standard deviation (error bars).

Figures:

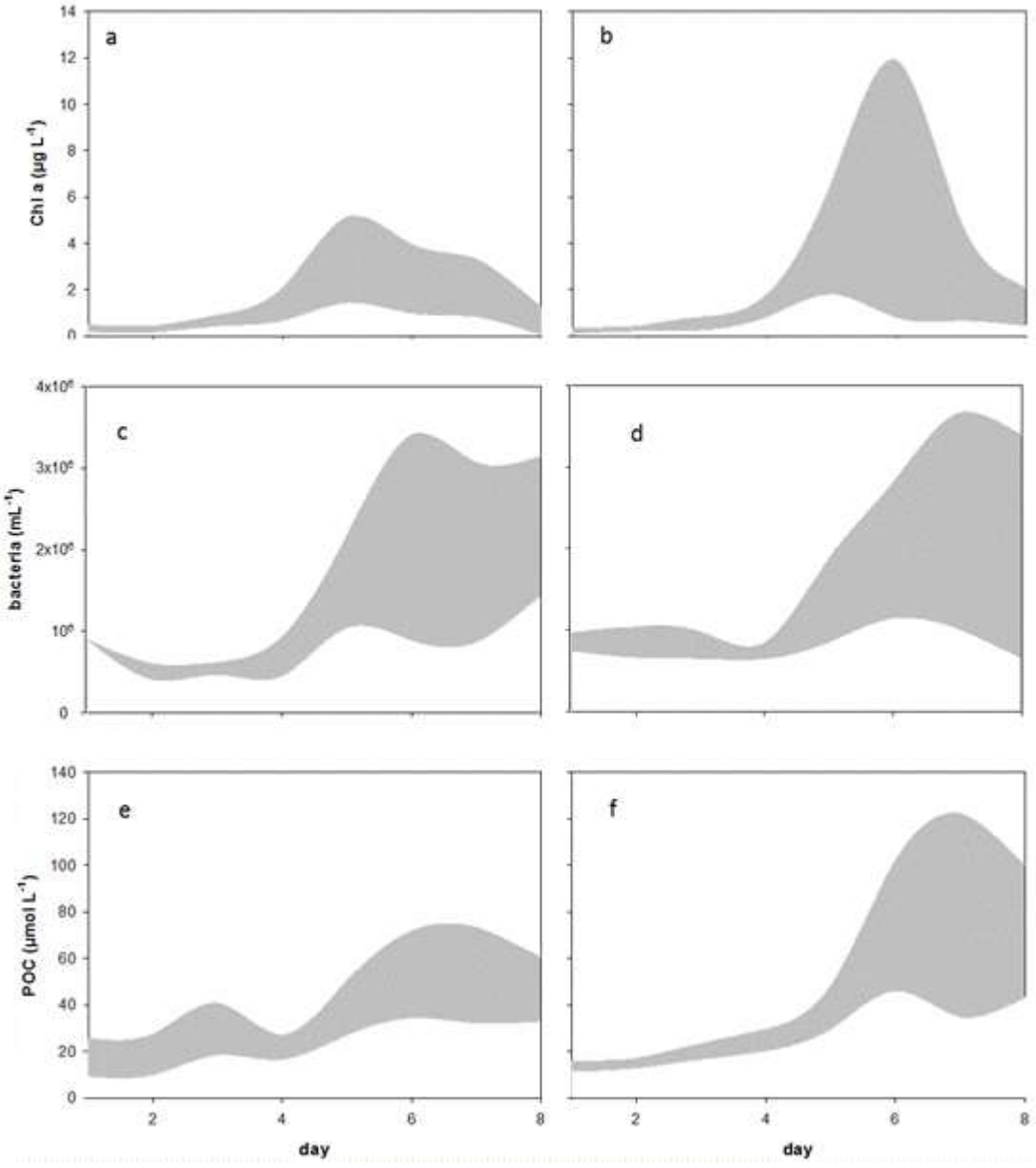

Figure: 1, a-f

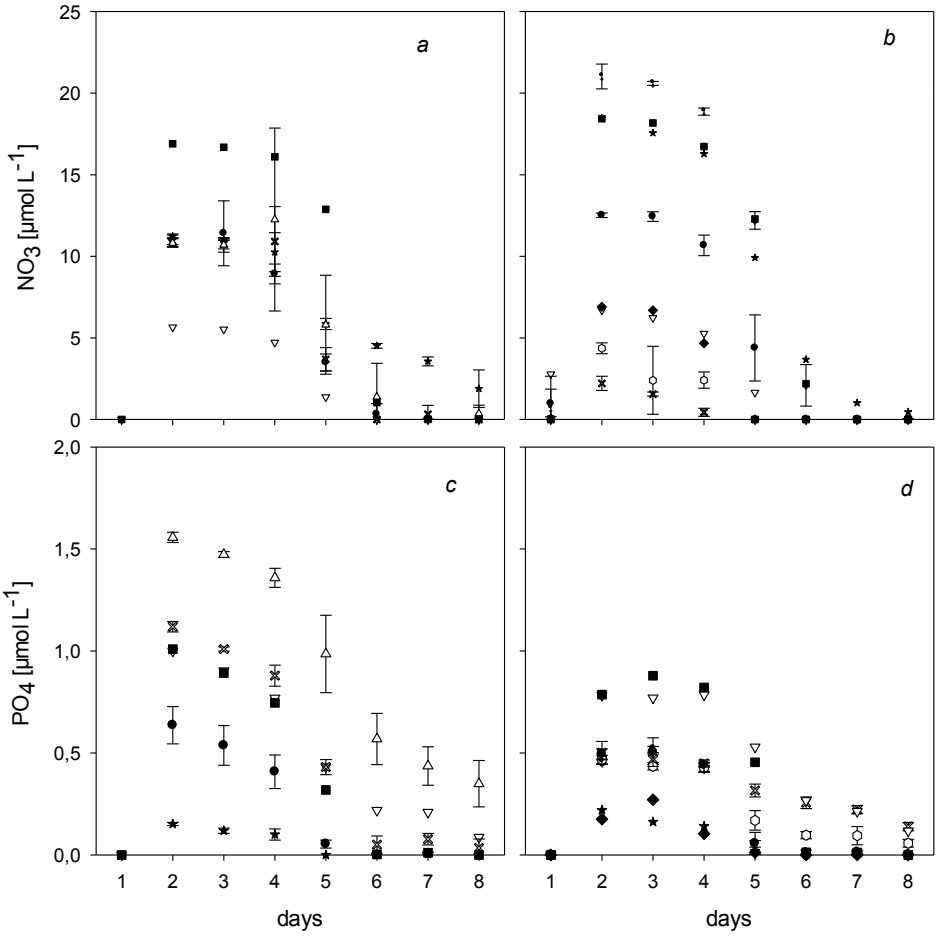
a
b
c
d
NO3 [µmol L-1]
PO4 [µmol L-1]
25
20
15
10
5
0
2,0
1,5
1,0
0,5
0,0
1
2
3
4
5
6
7
8
days
days

Figure: 2, a-d

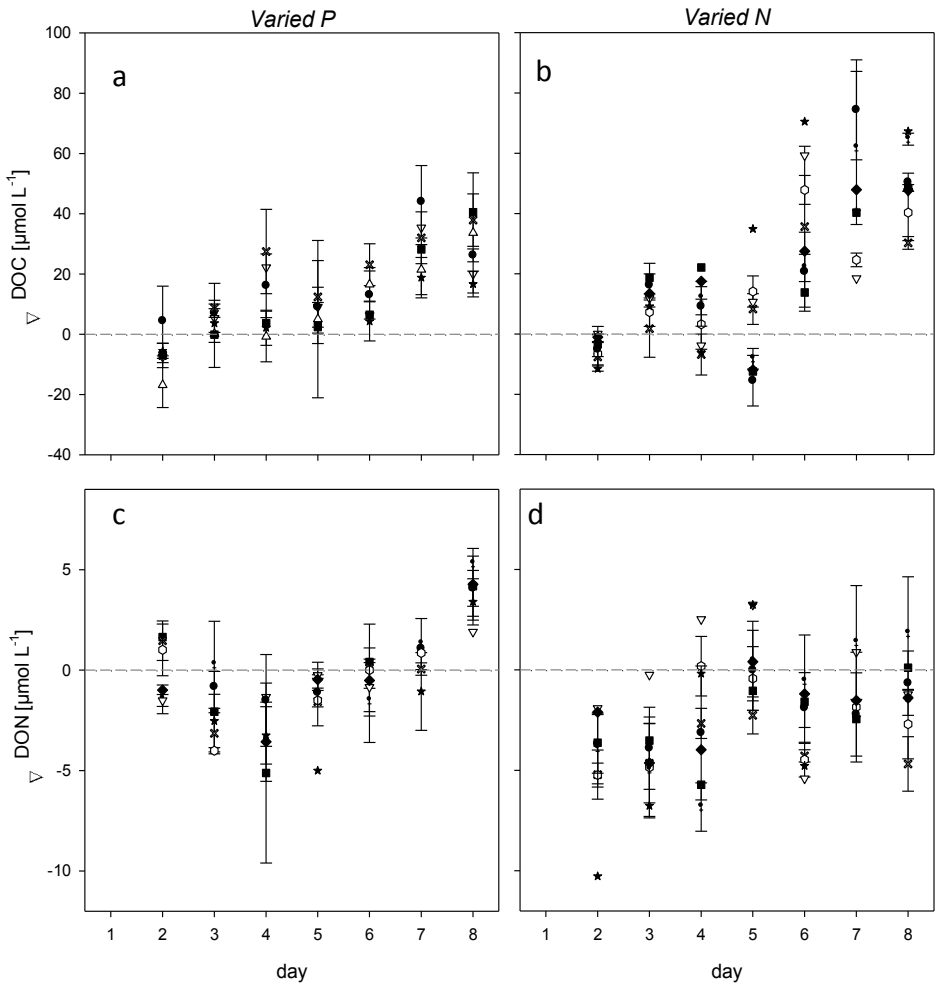

Figure: 3, a-d

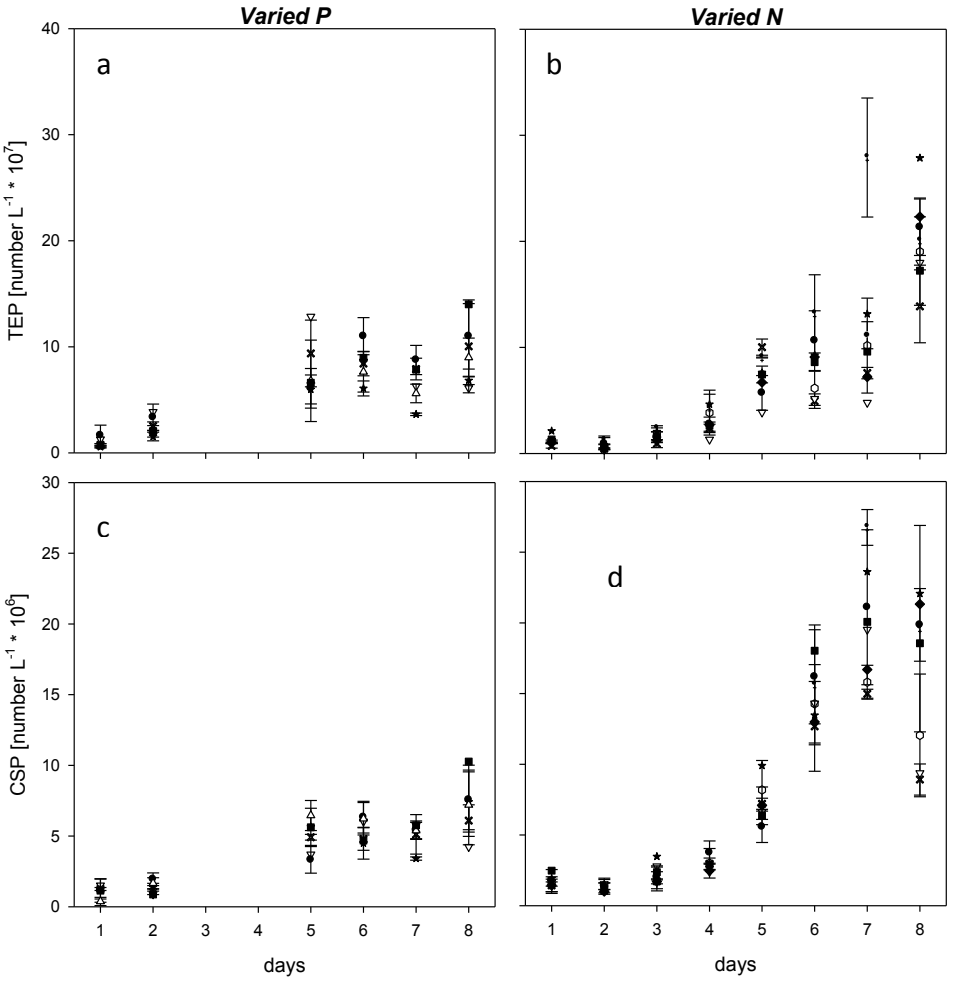
Varied P
Varied N
a
b
c
d
TEP [number L-1 * 10^7]
CSP [number L-1 * 10^6]
days
days

Figure: 4, a-d

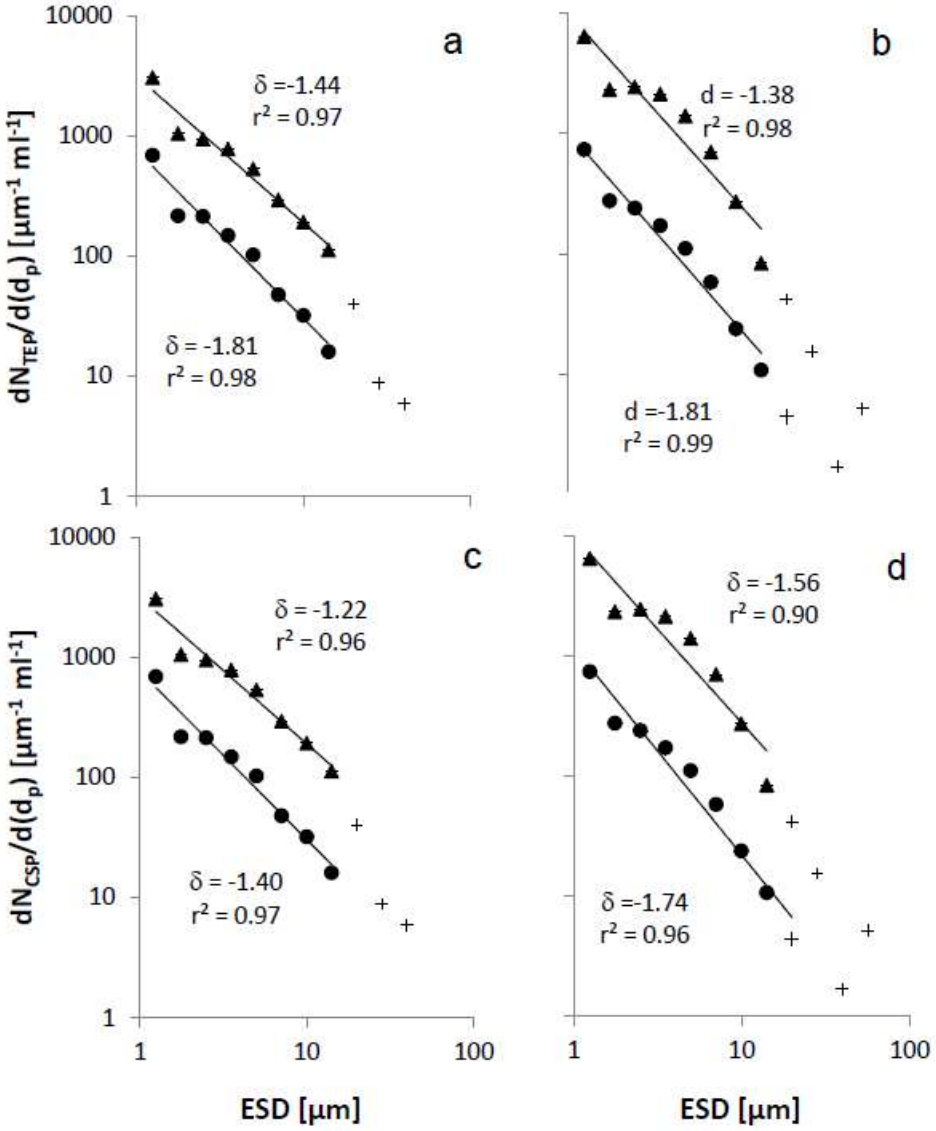
a
δ =-1.44
r² = 0.97
δ = -1.81
r² = 0.98
b
d = -1.38
r² = 0.98
d =-1.81
r² = 0.99
c
δ = -1.22
r² = 0.96
δ = -1.40
r² = 0.97
d
δ = -1.56
r² = 0.90
δ =-1.74
r² = 0.96
dN_TEP/d(d_p) [µm⁻¹ ml⁻¹]
dN_CSP/d(d_p) [µm⁻¹ ml⁻¹]
10000
1000
100
10
1
1
10
100
ESD [µm]
ESD [µm]

Figure: 5

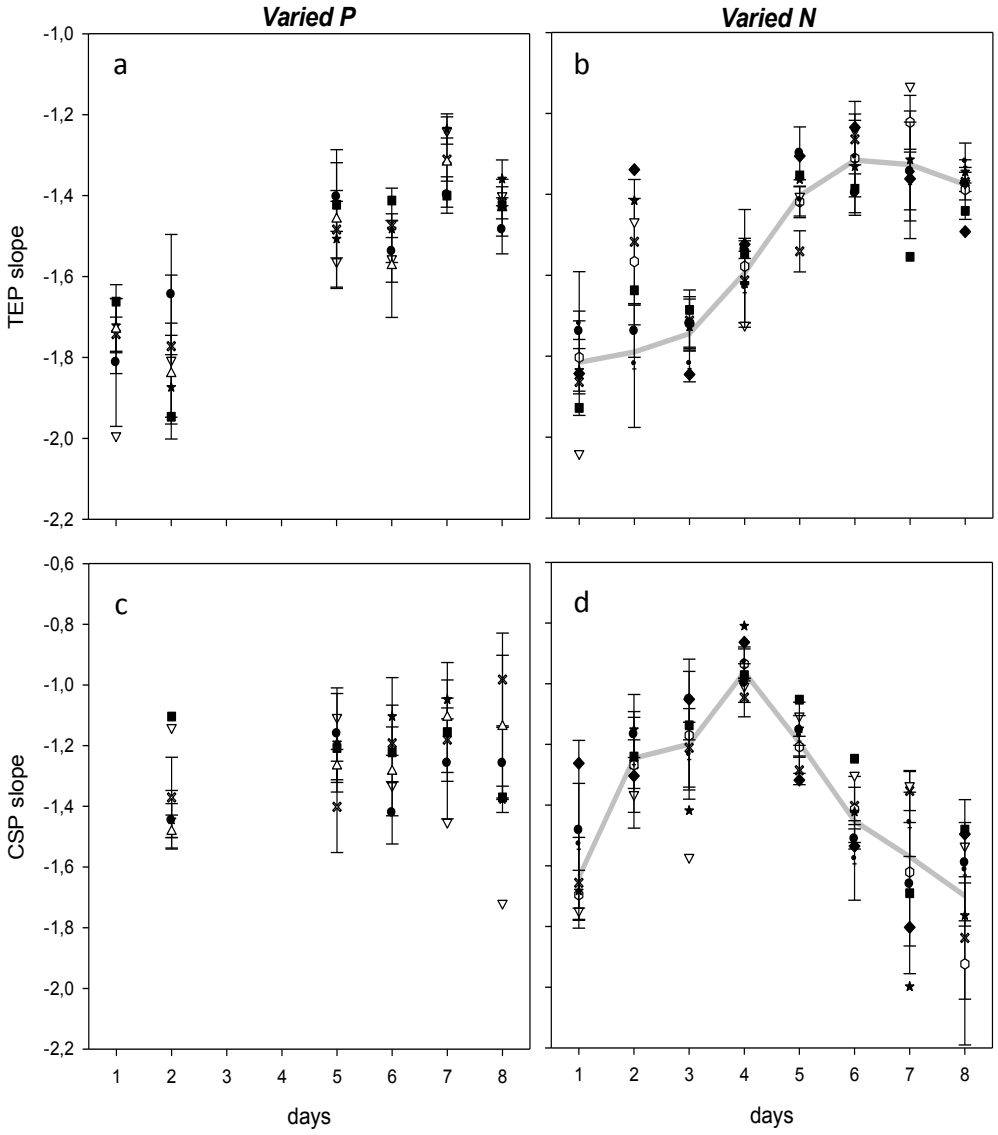
Varied P
Varied N
a
b
c
d
TEP slope
CSP slope
-1,0
-1,2
-1,4
-1,6
-1,8
-2,0
-2,2
-0,6
-0,8
-1,0
-1,2
-1,4
-1,6
-1,8
-2,0
-2,2
1
2
3
4
5
6
7
8
days
days

Figure: 6, a-d

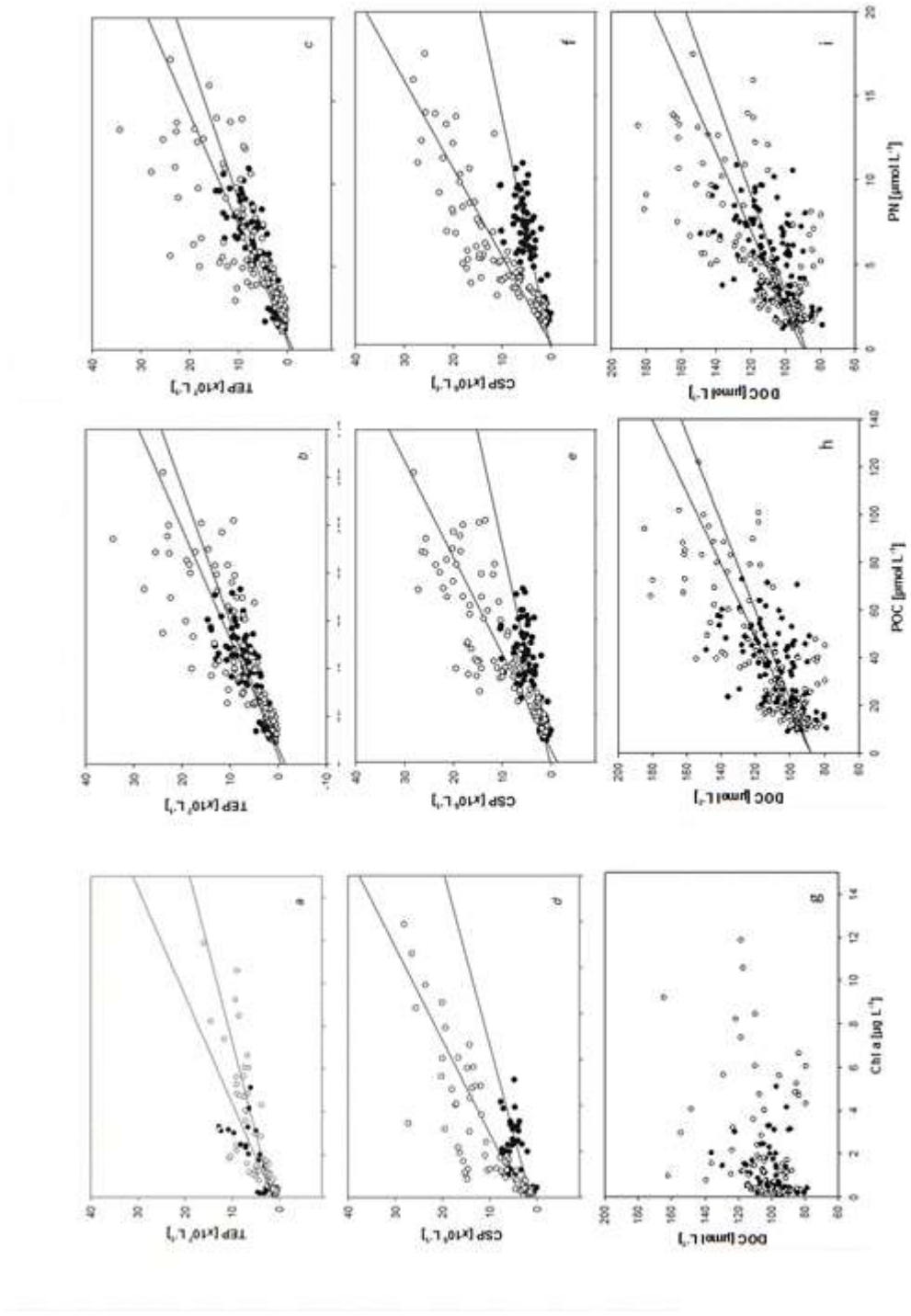
a
b
c
d
e
f
g
h
i
TEP [x10⁶ L⁻¹]
CSP [x10⁶ L⁻¹]
Chl a [µg L⁻¹]
DOC [µmol L⁻¹]
POC [µmol L⁻¹]
PN [µmol L⁻¹]

Figure: 7, a-i

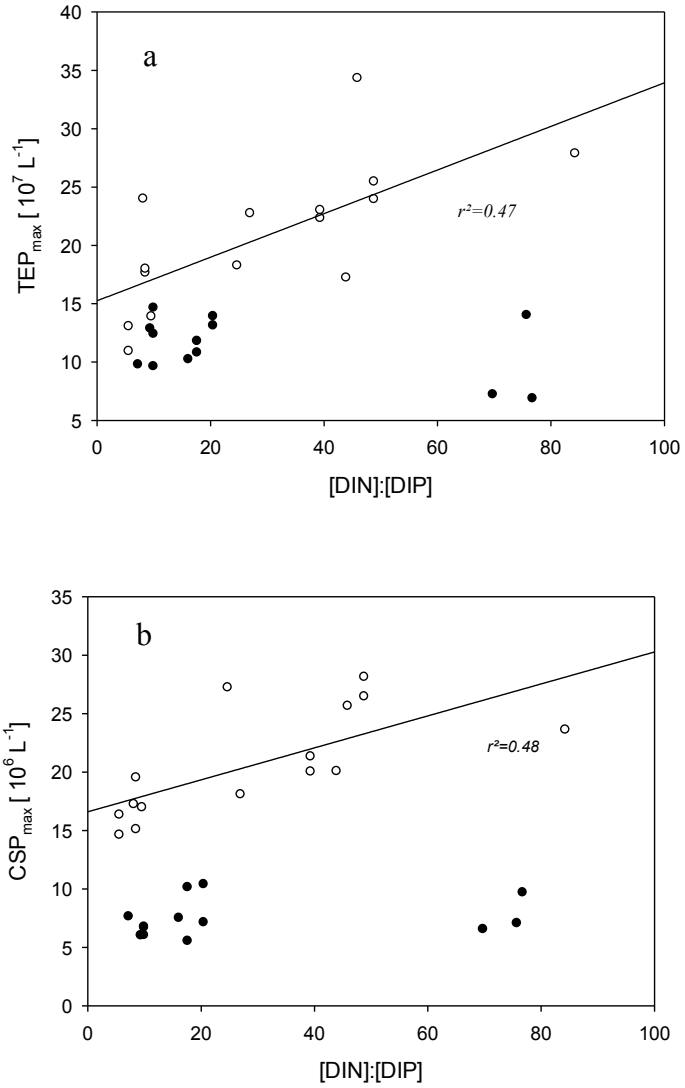

Figure: 8a, b

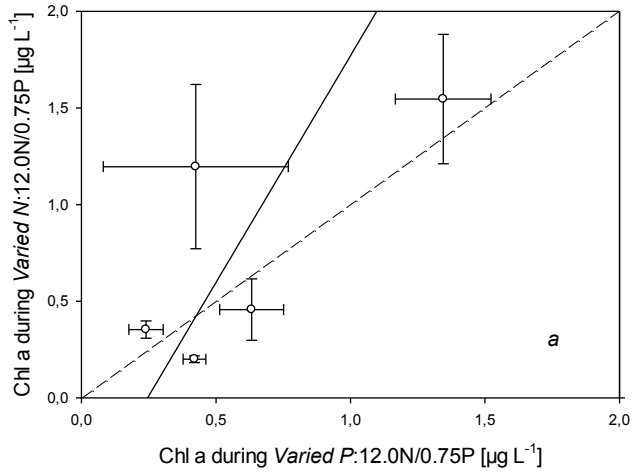
Chl a during *Varied N*:12.0N/0.75P [µg L^{-1}]
Chl a during *Varied P*:12.0N/0.75P [µg L^{-1}]
a

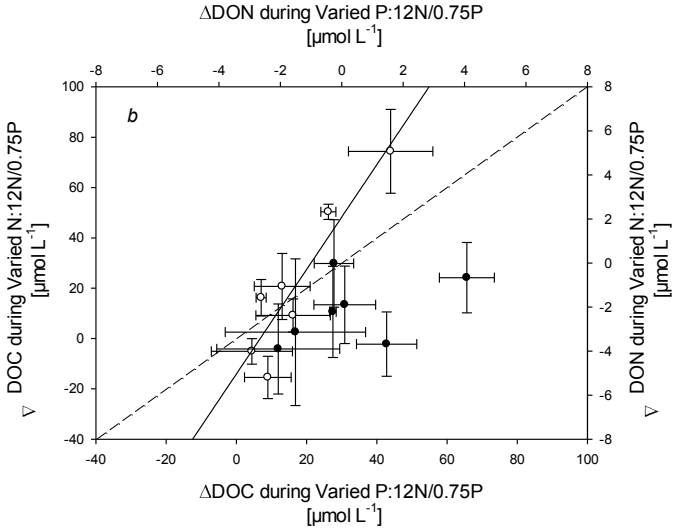
∆DON during Varied P:12N/0.75P
[µmol L^{-1}]
b
∇ DOC during Varied N:12N/0.75P
[µmol L^{-1}]
∆ DON during Varied N:12N/0.75P
[µmol L^{-1}]
∆DOC during Varied P:12N/0.75P
[µmol L^{-1}]

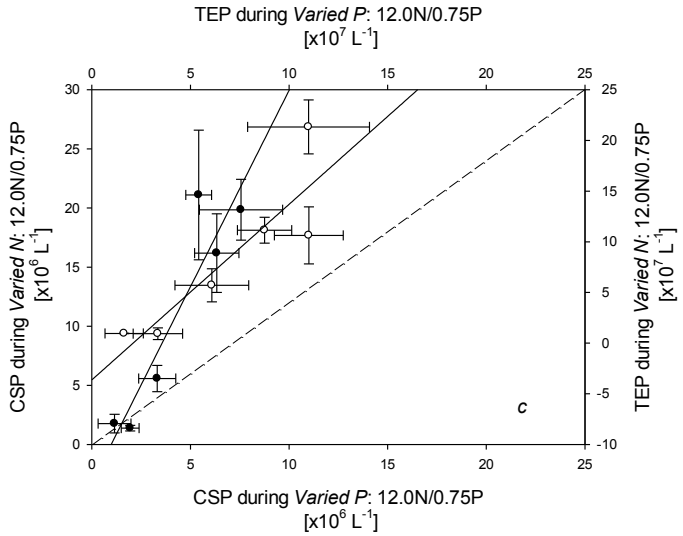
TEP during *Varied P*: 12.0N/0.75P
[x10^{7} L^{-1}]
CSP during *Varied N*: 12.0N/0.75P
[x10^{6} L^{-1}]
TEP during *Varied N*: 12.0N/0.75P
[x10^{7} L^{-1}]
c
CSP during *Varied P*: 12.0N/0.75P
[x10^{6} L^{-1}]

Figure: 9, a-c